UNCLASSIFIED

SECURITY CLASSIFICATION OF THIS PAGE

REPORT DOCUMENTATION PAGE

1a. REPORT SECURITY CLASSIFICATION: Unclassified	1b. RESTRICTIVE MARKINGS
2a. SECURITY CLASSIFICATION AUTHORITY	3. DISTRIBUTION/AVAILABILITY OF REPORT: Approved for public release; distribution unlimited
2b. DECLASSIFICATION/DOWNGRADING SCHEDULE	
4. PERFORMING ORGANIZATION REPORT NUMBER(S)	5. MONITORING ORGANIZATION REPORT NUMBER(S): AFOSR-TR. 86-0427
6a. NAME OF PERFORMING ORGANIZATION: Smithsonian Institution Astrophysical Observatory; 6b. OFFICE SYMBOL (If applicable)	7a. NAME OF MONITORING ORGANIZATION: Air Force Office of Scientific Research
6c. ADDRESS (City, State and ZIP Code): 60 Garden St. Cambridge, MA 02138	7b. ADDRESS (City, State and ZIP Code): Air Force Systems Command, USAF Bolling AFB, Washington, D.C. 20332
8a. NAME OF FUNDING/SPONSORING ORGANIZATION: AFOSR/NP; 8b. OFFICE SYMBOL (If applicable): NP	9. PROCUREMENT INSTRUMENT IDENTIFICATION NUMBER: AFOSR-81-0055
8c. ADDRESS (City, State and ZIP Code): Buidling 410 Bolling AFB, DC 20332	10. SOURCE OF FUNDING NOS. — PROGRAM ELEMENT NO.: 61102f; PROJECT NO.: 2311; TASK NO.: A1; WORK UNIT NO.: NA
11. TITLE (Include Security Classification): High Resolution Astrophysical Observations Usign Speckle Imaging	
12. PERSONAL AUTHOR(S): Dr. Noyes	
13a. TYPE OF REPORT: Final; 13b. TIME COVERED: FROM 1/1/81 TO 12/31/85	14. DATE OF REPORT (Yr., Mo., Day): 11 April 1986; 15. PAGE COUNT: 111
16. SUPPLEMENTARY NOTATION	
17. COSATI CODES — FIELD / GROUP / SUB. GR	18. SUBJECT TERMS (Continue on reverse if necessary and identify by block number): Speckle Interferometry: Speckle Imaging Solar Imaging: Photon-Counting Camera

19. ABSTRACT (Continue on reverse if necessary and identify by block number)

This report describes progress under a contract to develop a complete astronomical speckle image reconstruction facility and to apply that facility to the solution of astronomical problems. During the course of the contract we have developed the procedures, algorithms, theory and hardware required to perform that function and have made and interpreted astronomical observations of substantial significance.

A principal result of the program was development of a photon-counting camera of innovative design, the PAPA detector. Development of this device was, in our view, essential to making the speckle process into a useful astronomical tool, since the principal impediment to that circumstance in the past was the necessity for application of photon noise compensation procedures which were difficult if not impossible to calibrate. The photon camera made this procedure unnecessary and permitted precision image recovery.

20. DISTRIBUTION/AVAILABILITY OF ABSTRACT: UNCLASSIFIED/UNLIMITED ☒ SAME AS RPT. ☑ DTIC USERS ☐	21. ABSTRACT SECURITY CLASSIFICATION: Unclassified
22a. NAME OF RESPONSIBLE INDIVIDUAL: Henry Radoski	22b. TELEPHONE NUMBER (Include Area Code): (202) 767-4920; 22c. OFFICE SYMBOL: NP

DD FORM 1473, 83 APR — EDITION OF 1 JAN 73 IS OBSOLETE.

Unclassified

SECURITY CLASSIFICATION OF THIS PAGE

DTIC ELECTE JUL 31 1986 D

DTIC COPY

AD-A170 430

86 7 23 093

19. Abstract (continued)

The result of this effort and the associated algorithm development was an active program of astronomical observation which included investigations into young stellar objects, supergiant structure and measurements of the helium abundance of the early universe. We have also continued research on recovery of high angular resolution images of the solar surface working with scientists at the Sacramento Peak Observatory in this area.

AFOSR-TR- 86-0427

AFOSR-81-0055

High Resolution Astrophysical Observations Using Speckle Imaging

ROBERT W. NOYES
PETER NISENSON
COSTAS PAPALIOLIOS
ROBERT V. STACHNIK

Smithsonian Institution
Astrophysical Observatory
60 Garden Street
Cambridge, MA 02138

11 April 1986

Final Report
1 January 1981 - 31 December 1985

APPROVED FOR PUBLIC RELEASE; DISTRIBUTION UNLIMITED

AIR FORCE OFFICE OF SCIENTIFIC RESEARCH
AIR FORCE SYSTEMS COMMAND
UNITED STATES AIR FORCE
BOLLING AIR FORCE BASE, WASHINGTON, D.C. 20332

INTRODUCTION

Under this contract we have developed a complete high resolution speckle imaging facility and have used that facility to produce a range of results of both scientific and technical significance. Among the results of our efforts have been the following:

- Development of a new camera, the PAPA detector, a high-speed photon counting/photon cataloging sensor which appears to be exceptionally well suited to speckle and other imaging problems, and of an advanced front end package.

- Development of a high-speed/high capacity digital videocassette data recording system.

- Development of a speckle imaging test bench.

- Development of a dedicated speckle data processing facility, for stripping, processing and display of speckle imagery.

- Development of a range of new algorithms for speckle imaging.

- Development and characterization of an image-intensified CCD camera for solar surface observations.

- Discovery of a very faint visible companion to the prototype Young Stellar Object T Tauri. The new source is located due north of T Tauri A and is distinct from the recently discovered infrared source, which is due south of T Tauri A.

- Discovery of two stellar companions to the bright supergiant star Alpha Orionis. The innermost companion appears to have a significant effect on modulating the observed properties of the supergiant and, as it orbits inside the chromosphere of Alpha Ori, may play a major role in governing the details of the latter's mass loss behavior.

- Detection of the faint optical companion to mu Cassiopia, an old halo population star whose helium abundance is believed to reflect that of the primordial universe. Our observations are the most precise to date and the first in the visible. Inadequate astrometric and parallax data make accurate helium abundance determination impossible, but, by the time accurate space-based parallax measurements are available, our new orbit will permit helium abundance determination precise enough to discriminate between early universe theories.

- Serendipitous discovery of a number of binary stars with exceptionally large magnitude differences.

Many of these developments are described in the published papers which form the major part of this report, as appendices. Brief descriptions of accomplishments in important subareas appear in the following pages.

THE PAPA DETECTOR AND THE NEW FRONT END PACKAGE

The first working version of the PAPA (Precision Analog Photon Address) detector, a new two dimensional photon counting camera, has been built with substantial support from this contract. The camera has now been used on several data collecting runs on large telescopes, and produced a growing body of scientific results, some of which are discussed in this report. A description of the present version of the detector has been published in Applied Optics (January, 1985). The camera has 512x512 pixels and can record positions for up to 100,000 photons per second. The quantum efficiency of the detector is determined by the front end image intensifier. The high gain Gen II front end has a very low quantum efficiency, only about 3% at peak, due to losses at the channel plate. This compares to quantum efficencies exceeding 15% for Gen I tubes.

A new version of the PAPA is currently being built for us by Adaptive Optics Associates. Several major changes in the design and construction of this unit should yield a camera which has substantially enhanced characteristics, compared to the original version. A new image intensifier package which couples a Gen I tube to the front of a Gen II should improve the quantum efficiency to 12% or higher. Improved transfer optics should have less aberration and yield larger pulses per detected photon to the photomultipliers. This should result in a reduction in the number of mistakes that the camera makes in photon position. An extra pair of fine masks in two additional channels will allow digital interpolation of pulse heights and an increase in the camera resolution by as much as a factor of eight (4096x4096). Improved high speed electronics will increase the maximum count rate of the camera to over 1,000,000 per second and care has been taken to improve the thermal stability of the preamps which had, in the previous version, a tendendancy to drift slowly, resulting in changes in thresholds and increases in address errors with time. Finally, the mechanical structure has been redesigned into a much more compact package, increasing the flexibility of application for the detector.

A new computerized front-end package has been designed, built and used for observing. This package contains an automated atmospheric dispersion corrector (counter-rotating Risley prisms), filters, stops, magnification optics and a 1:1 imaging lens for field finding with the PAPA. The unit has a single board computer which accepts Basic commands from the main control computer. It has proved to be extremely efficient in optimizing an observing program, since no manual intervention is required. Its first use was at the CTIO observatory in Chile, where it worked flawlessly, producing many hours of good data. It has been built with a universal flange and coupling so it can take either the old or the new PAPA detector.

DEVELOPMENT OF A LABORATORY ATMOSPHERIC OPTICS SIMULATOR

An early program goal was development of a contolled laboratory environment within which high resolution imaging hardware and software could be tested and quantitatively evaluated. This is a task which is straightforward in principle but can be difficult in execution.

The laboratory simulator is located in a dedicated instrument developent laboratory and allows us to produce an image of a target, distorted by random phase errors in an intermediate pupil plane, at the input to the front end package. The front end package normally mounts to the telescope bolt circle and relays a spectrally-filtered, magnified and atmospherically-dispersion-corrected image to the sensor. The ratio of "atmospheric correlation distance" to pupil diameter, correlation time and exit focal ratio can be varied to simulate a variety of observing conditions.

It is difficult to overstate the value of this facility in allowing us to test new instuments, software and processing procedures in a laboratory environment.

DEVELOPMENT OF A DEDICATED SPECKLE PROCESSING FACILITY

Early speckle data analysis was performed using mainframe computers at Harvard or Smithsonian. The advantages of having our own dedicated facility, in terms of turn-around-time and ease of access, quickly became apparent.

With very significant help from AFOSR, as well as other sources, we have established our own computer facility consisting of a DEC PDP 11/34 with array processor, a Data General Nova 1200 and a DEC microVAX II, all with supporting disks and eight terminals, 3 tape drives, a Versatec printer/plotter, a continous-tone image display, as well as high speed data lines to two DEC VAX 780s, a DEC 8600, and all the associated peripherals and supporting specialized utilities of those machines. Four microcomputers are used in instrument control and some small-scale data analysis applications.

All elements of the system are very heavily used with overnight processing runs common. The heavy computing and data analysis requirements of speckle imaging are exceptionally well served by this facility.

ALGORITHMS FOR SPECKLE IMAGING

Some work has been done in characterizing the noise in speckle interferograms taken with the PAPA detector. It was found that the photon-camera data is well described by a simple theory which predicts the SNR for each frame of speckle data. The SNR for each frame is a function of the normalized speckle power spectrum and the number of photons per frame. Quantum limited performance is achieved when the number of photons per speckle varies over four orders of magnitude, from 20 to .002.

The SNR for an integration of many frames is then presumably given by the SNR per frame scaled by the square root of the number of frames. One can frame the data with different exposure times and estimate the SNR that results for the integration. We find that the SNR varies slowly with the frame time, a result predicted by Dainty and O'Donnell, and that the optimum frame time varies from

10 to 40 ms depending on the conditions.

We have investigated two iterative algorithms for deconvolving the blurring introduced by the atmosphere. The first is a constrained iterative deconvolution algorithm which stably recovers the high frequency content of a blurred image given the long exposure images of the blurred object and a point-like reference star. This algorithm has been used extensively to deconvolve spectroscopic data but we could find no evidence of its application to noisy 2-D images. In a series of simula- tions, we showed that it could stably recover point-like and extended images even with ~ 10% photon noise per pixel. However, it converges slowly and is only useful when the blurred image already exhibits significant structure.

The second algorithm is novel and provides a means of estimating the object's power spectrum or autocorrelation. It is based on the notion of alternating projections onto convex sets and is a generalization of Gerchberg-Saxton type algorithms. It starts with an estimate of the power spectrum that is similar to a Wiener filter estimate. The iterate alternates between autocorrelation and power spectrum domains. In each domain, various constraints are imposed that force the iterate towards a physically realizable estimate that is consistent with the data. The power spectra that result are smooth out to frequencies higher than the initial estimate and the autocorrelations are much cleaner than the initial estimate and have none of the oscillations that characterize linear estimates. We intend to use the reweighted power spectra this algorithm provides in conjunction with phases from Knox-Thompson in order to produce speckle images.

We have also begun to re-examine the iterative algorithm we currently employ to recover the Knox-Thompson phases in hopes of improving its performance with noisy data. We have found that with data as noisy as we typically get from the PAPA, a two-path estimate of the intial phase appears to be worse than assuming that the object has zero phase. In addition, we have discovered that the iterative algorithm can never take out a phase ramp (a shift in image space), and converges slowly when the predominant error in the iterate is a phase ramp. We are in the process of modifying the iteration to account for these difficulties.

LOW LIGHT LEVEL SOLAR IMAGING

A program for producing high angular resolution images of solar surface features has been supported by both this contract and a contract by AFGL and the Sacramento Peak Observatory (SPO). The major effort in the AFGL program was broadband speckle imaging while the emphasis in this program was imaging in spectral lines at much lower light levels. Both projects required the use of our our Photometrics CCD system, which utilizes a thick RCA chip (512x320) having insufficient sensitivity for direct narrow wavelength band data recording, particularly in the blue spectral region. Since many of the most interesting solar imaging problems require observations in the Ca II or H alpha region of the solar spectrum, this is a severe limitation. It was hoped that reimaging the output face of a blue sensitive image intensifier onto the CCD would solve this problem. Two data gathering runs were carried out in 1984, one at the National Solar Observatory McMath 60" telescope,

and the other at SPO. While data recording appeared to be successful and integrated images looked potentially interesting with much fine detail observable, the speckle image reconstruction processes did not produce images of a quality comparable to the broadband reconstructions generated from direct CCD imaging in earlier observations.

The problems in the reconstruction process appear to be similar to ones encountered when data were recorded with the ISIT video system: correction of the photon noise bias cannot be performed with sufficient accuracy. In low light level data sets, the signal of interest sits on a bias whose amplitude is proportional to the number of detected photons, and whose shape is determined by the point response of the detector. The fainter the detected source, the larger the ratio of bias to signal and the greater the accuracy of correction required. With a photon counting camera such as the CfA PAPA detector, this noise bias may be corrected exactly since the number of detected photons is known, and each photon is detected as a delta function. With the intensified CCD system, the number of photons must be estimated from the power spectrum of the data itself, and the detected photon shape is determined from the combined point spread functions of the intensifier, optical relay system and the CCD. In the high light level regime in which the CCD is used directly, he photon noise bias level is very small, so no correction is required. However, the intensified data increases the bias level by several hundred times. Estimates of the bias shape were produced using low light level flat fields recorded at the time of data acquisition. However, inaccuracies in these estimates appear to be too great, and substantial degrading effects of the noise bias remain in the reconstructions, despite our best efforts to eliminate them.

The most promising solution to the low light level problem is to use a more sensitive detector for the narrow band experiments. New CCD chips generated by Tektronics have two orders of magnitude more sensitivity than the RCA chip, and also have greatly improved blue response without suffering the interference fringing effects which have been a problem with other thinned chips. These CCDs should be usable without intensification, and substitution of a new chip in the Photometrics camera system should be straightforward. For very narrow, very low light level imaging, use of the PAPA detector may be possible. However, for flux levels at which the PAPA is not saturated, integration times needed for high signal-to-noise reconstructions may well exceed the expected time stability of the solar features.

THE T TAURI OPTICAL SOURCE

Discovery of a radio and infrared companion to the young stellar object T Tauri led us to undertake a search for this companion at optical wavelengths. As expected, the low temperature of the companion made it undetectable in the visible, however a new source was found. Located 0.27 arcseconds from T Tauri A, at a position angle of 358 $\pm$ 5 degrees, the faint optical source is located on the opposite side of the primary from the radio/infrared object, which is to the south and about 0.61 arcseconds from the bright optical source. The visual magnitude difference between the new northern component and the primary is 5.3 $\pm$ 0.2 magnitude at 450 nm. This very great difference in brightness made detection unusually difficult and the

measurements not only shed light on the structure of the T Tauri system but also demonstrate the power of the camera. The ability to produce images was essential to arriving at our interpretation of the data since, given the 180 degree ambiguity associated with simple speckle interferometry, there would have been a strong temptation, in the absence of other knowledge, to associate the new source with the previously-known IR/radio object.

Based on its high luminosity and apparently thermal spectral distribution, we have identified the northern star as a low mass star. The in-line configuration of the three objects is highly suggestive, however. Many T Tauri and other young stellar objects display oppositely-directed jets and bullets. In a model due independently to both Appenzeller and Strom, such structures should be associated with dust disks and be oriented normal to those disks. Bullets or condensations in the jets would, for the oncoming jet, be relatively unobscurred, while, for the receeding jet, would be heavily reddened, becoming invisible at optical wavelengths. While the luminosity of the visible source argues against this interpretation, the similarity between the model predictions and what we see is striking. Also striking is the fact that the geometry of the system is at odds with what one might expect for a typical multiple star system. Two coincidences appear to be present. One is the high degree of alignment for the radio, bright optical and faint optical souces - within 5 degrees. The second is the circumstance of a 2:1 ratio of projected separations. Dynamics of triple systems do not allow stable orbital spacing ratios smaller than 5:1, and they are generally much larger. A 2:1 ratio requires convenient projection angles. There is no reason such coincidences cannot be present but their existence suggests that additional observations would be valuable in clarifying the nature of the system.

Proceeding with the assumption that the new visible source was a star, we also assumed that both stars had the same extinction and that, to first approximation, they could be represented as black bodies in order to deduce a probable spectral class for the northern companion. Using the measured magnitude differences as a function of color and an estimated color temperature for T Tauri A of 5000K, the estimated temperature of the companion is 3000K $\pm$ 200, corresponding to spectral types in the range M4 to M8. Using the PMS convective-radiative evolutionary tracks of Cohen and Kuhi suggested that an appropriate mass for the new northern companion would be approximately 0.35 Msun making this star one of the least massive pre-main sequence stars yet detected.

OBSERVATIONS OF ALPHA ORIONIS

Two optical sources in proximity to the red supergiant α Ori were detected at the Steward Observatory 2.2 meter telescope in November 1983. The observed separation for the more distant source was found to be 0.51 $\pm$ 0.01 arcsecond, and for the closer 0.06 $\pm$ 0.01 arcsecond.) This observation was consistent with an earlier detection of two sources in 1982. The new position of the close optical source has changed from the previous observation, while the two measurements of position angle and separation of the distant companion coincide within the errors of measurement. The magnitude differences with respect to the primary, measured at 656.3 nm (H α) and 656.8 nm (red continuum), are 3.0 and 3.4 respectively, for the close companion, and 4.3 and 4.7 for the distant source.

The high brightness of the two sources, compared to α Ori, (in H α as well as in the continuum), suggests that they may be stellar companions to α Ori. Given our limited information on color dependence it is very difficult to determine spectral classes for the companions.

Supporting evidence for the existence of a close stellar companion was found in polarization data for α Ori. We detected a periodicity of about 2.1 years in measurements of the position angle of the plane of polarization. The amount of polarization appears to manifest periodicity as well. The period is approximately half of that which has been detected for the position angle. Also the variations in the degree of olarization seem to be in phase with the photometric variations of α Ori.

Our analysis of polarization as a function of wavelength (data accumulated by different observers during the period from 1968 through 1984) shows $1/\lambda$ dependence characteristic of Mie scattering by dust grains. We are led to a picture in which the observed polarization is a consequence of a large-scale asymmetry created by the close companion orbiting α Ori inside its extended dust envelope.

Modeling the polarization data permitted determination of a plausible orbit, which also matches the interferometric data. This orbit is defined by following parameters: $P = 2.1$ yrs, $T = 1980.4$, $a = 4.7$ a.u., $e = 0.35$, $i = 30°$, $\Omega = 60°$, $\omega = 0°$. From Kepler's third law, the inferred sum of the masses of α Ori and the close companion is 24 M_o. Assuming a mass of 20 M_o for α Ori the estimated mass of the companion is about 4 M_o.

We used the previously determined orbit to predict the positions of the companion for the two epochs when Goldberg *et al.* and Roddier and Roddier observed bright features on the stellar limb. The position angle of the bright feature observed by Goldberg *et al.* is 208° ± 5 and Roddier and Roddier 202° ± 5. The predicted positions are 214° and 195°, respectively. Since the predicted and measured position angles are very similar, we suspect that they actually may have observed the close companion.

Our orbit predicts that the companion passes only half a stellar radius from the surface of the supergiant. This corresponds to an angular separation of 0.03 arcsecond. Assuming a stellar distance of 95 parsecs, the linear separation of the companion will be 3 a.u. We expect to see interesting phenomena when the companion is so close to the photosphere of a red supergiant. Among the possibilities are: formation of large convective structures on the surface of the supergiant, tidal distortion of the primary, mass ejection from the primary, and possibly, formation of an accretion disc or envelope around the companion.

Goldberg pointed out that during the last 60 years an unusually large, rapid decrease in the radial velocity of α Ori occurred several times. He suggested that this might be connected with the star's pulsation; instabilities in the atmosphere could trigger mass ejection and the formation of dust grains.

In order to examine a possible connection of these instabilities with the orbital motion of the close companion, we compared the epochs of the large decrease in radial velocity with the corresponding epochs of the companion's periastron passage. The epochs we determined from the data presented by Goldberg are: 1926.6, 1938.8,

1944.9, 1961.5, 1978.3 (± 0.2 yrs). The predicted epochs are: 1926.3, 1938.8, 1945.0, 1961.6 and 1978.3 (± 0.1 yrs). The fact that such events do not appear during each periastron passage could be explained if mass ejection occurs only when the epoch of periastron is just after the maximum velocity of pulsational expansion.

The outbursts which probably took place in 1944.9, 1961.5 and 1978.3 have been identified by Karovska as likely origins of the expanding shells observed at about 45 stellar radii by Bloemhof, at 17 stellar radii by Honeycutt, and 2.5 radii by Roddier and Roddier, respectively. The shell at 2.5 stellar radii was observed in November 1980, and was also detected at 3.5 radii in February, 1982 by Karovska, showing an expansion with mean velocity of about 5 km/s.

OBSERVATIONS OF MU CASSIOPIA

Mu Cassiopia is an population II halo star believed to be among the oldest stars in the galaxy. Since the helium abundance of old stars may reflect the helium abundance of the primordial universe, and because this parameter can be used to distinguish between competing theories of early universe formation, it is of great interest to learn the helium abundance of population II objects. This is difficult because the only stars which have lasted long enough to be visible today are those which are quite cool, too cool to show helium in the spectrum directly. It was recognized by Dennis that the theory of stellar interiors was sufficiently advanced that a mass and luminosity, alone, for a population II star would allow inference of a helium abundance but that only one star was known for which there was a reasonable chance of obtaining a mass. This was the star mu Casssiopia, a 22 year period astrometric binary.

The astrometric observations suggested that mu Cas was a subarcsecond separation binary with a magnitude difference greater than 5. Astrometricly-determined orbital elements were sufficient to determine a mass fraction but not a sum of the masses. This latter quantity could be determined only from measurement of the physical separation of the components, requiring a parallax and an angular separation. Numerous investigators have attempted to measure angular separations with varying degrees of success.

As pointed out by Faulkner, the accuracy in estimation of the fractional helium abundance required for cosmological purposes is about 0.1. This implies knowledge of the semimajor axis to within 3 or 4 percent. McCarthy, like Pierce and Lavery, concluded that the dominent source of error in earlier attempts to deduce helium abundances for mu Cas A was inaccuracy in the astrometrically-determined orbital elements. However, discrepencies between measurements made by those two observers, who worked in the infrared where magnitude differences are less extreme, suggest that improvement of the astrometric orbit is not the only way to constrain the helium abundance. More accurate measurements of of the position angle, separation and magnitude difference for mu Cas B are necessary.

Our measurements represent the first visible wavelength (850 nm) detection of mu Cas B. At the epoch of observation, we found a separation of 0.118 ± 0.045 arcseconds at a position angle of 63 ± 2 degrees. The magnitude difference was 4.96 ± 0.17, leading to a magnitude difference as 550 nm, where the astrometric studies were done, of 6.78. Using Lippencott's astrometric orbit and parallax we obtain helium abundances of 0.21 ± 0.17 for a metallicity of 0.005 and 0.29 ± 0.17 for a metalicity of 0.015. The lower metalicity is probably most appropriate.

This work demonstrates that we are now in a position to move quickly to derive our own orbital elements from a program of careful speckle observations of mu Cas. With new determinations of parallax which should come from Hipparchos or Space Telescope observations within the next few years, we expect to provide definative measurements of the mu Cas helium abundance on that time scale.

SERENDIPITOUS DISCOVERY OF BINARY STARS

Our observing program has been directed toward study of a range of objects for which we wished to obtain answers to specific scientific questions and has not been oriented towrad survey-type programs. Nevertheless, primarily in our inspection of stars intended to serve as point-like reference sources, we have found a significant number of objects which are, in fact, double. While we hae cataloged these objects, we have not yet published a listing of these newly-discovered binaries.

Some of our discoveries of multiple structure in program stars have had important implications for understanding the physics of the systems involved, but this has been the case for some reference stars as well. As an example, we have determined that two of the most commonly used reference stars for alpha Orionis, gamma Orionis and delta Orionis, are, themselves, binary. This has not previously been reported, we believe, because, among commonly used camera systems, only the PAPA detector has the dynamic range to see the companions.

SUMMARY AND CONCLUSIONS

Under this program, we have successfully built up a high spatial resolution imaging capability around two areas of technical development unique to our program: advanced imaging algorithms based on the Knox-Thompson procedure for phase recovery and the PAPA detector, which provided us with high quality low light level imagery. Technical assets, developed under the program, which also are also unique elements of our effort include a portable, high-data-rate videorecorder-based digital data recording system and a flexible, dedicated image processing laboratory.

Scientific results of the program include serendipitous detection of binary stars and direct imaging of calcium line features on the solar surface using the intensified CCD. Major scientific results include detection of a faint visible companion to the prototype Young Stellar Object T Tauri, discovery of two companions to the supergiant alpha Orionis, one of which is believed to play a significant role in modulating

the gross observable properties of the system, and the first visible detection of the very faint companion to the old halo population star mu Cassiopia, which may allow computation of a helium abundance reflecting that of the early universe.

APPENDICES

A partial collection of (recently published) research papers.

A - Speckle Imaging with the PAPA Detector

B - Digital Recording on Video Cassette

C - Constrained Iterative Deconvolution of Noisy 2-D Images

D - Signal-to-Noise in Photon Counting Speckle Interferometry with Real Detectors

E - A New Optical Source Associated with T Tauri

F - The Companions to α Orionis

G - Optical Speckle Imaging of μ Cassiopiae

APPENDIX
A

Reprinted from Applied Optics, Vol. 24, page 287, January 15, 1985

Speckle imaging with the PAPA detector

Costas Papaliolios, Peter Nisenson, and Steven Ebstein

A new 2-D photon-counting camera, the PAPA (precision analog photon address) detector has been built, tested, and used successfully for the acquisition of speckle imaging data. The camera has 512 × 512 pixels and operates at count rates of at least 200,000/sec. In this paper we present technical details on the camera and include some of the laboratory and astronomical results which demonstrate the detector's capabilities.

I. Introduction

A new 2-D photon-counting camera has been built and successfully used for speckle imaging. The PAPA (precision analog photon address) detector works well at count rates of at least 200,000/sec and has 512 × 512 pixels of resolution. It provides a list of photon addresses in the order of their detection and can supply their arrival times to a precision of ~1 μsec. An earlier version of this camera[1] was built and provided the experience that enabled the construction of the present highly successful model. The camera has been tested in the laboratory and now has been used on three telescope observing runs.

The properties that make this camera particularly useful for speckle work are (1) the individual photon positions are recorded making it possible to do exact photon noise bias corrections that arise from the quantization of the detected signal[2]; (2) the time information allows tailoring of the frame time (equivalent to the exposure time for a conventional camera) to match the atmospheric correlation time when the data are being computer processed, resulting in an optimized signal-to-noise ratio; (3) recording the addresses of the detected photons is much more efficient than recording the number of photons in each pixel position (as with an array detector), since there are only a few photons detected per frame, for faint objects.

In this paper we present a status report on the current state of the PAPA detector, along with results of tests in the laboratory and speckle data acquisition at the telescope. Potential improvements in the maximum count rate and spatial resolution of the camera are discussed as well as its application to other areas.

II. Speckle Imaging

Speckle interferometry is a technique, first used by Labeyrie,[3] that eliminates the atmospherically caused degradation in resolution which plagues all ground-based telescopes with apertures larger than ~10 cm diam. Speckle imaging, an extension of this technique,[4,5] results in full image reconstruction at the diffraction limit of the telescope. The data taking requirements for both imaging and interferometry are quite similar. A sequence of short exposure photographs taken with a large telescope provides the basic input data. The exposure time is set to approximately match the atmospheric correlation time, typically 10 msec, but which may vary by an order of magnitude depending on the site and the atmospheric conditions. Because of this short exposure time and the narrow spectral bandwidths (~100 Å) that are needed there are very few photons per exposure. The number of photons becomes even smaller for fainter objects, which always seem to be the most interesting ones to study. Although the processing of the data in the pioneering work of Labeyrie was done photographically using analog methods, these methods are inadequate and not very flexible for the present objects of interest. The information in each exposure is now entered into a digital computer which performs the speckle processing.

We initially tried to provide the data required for our speckle program with an intensified film camera and later with an intensified video camera (an ISIT). Both cameras were only partially successful in providing data on the faint objects we were most interested in. It became apparent that the ideal camera for our purposes would be one that would detect individual photons as delta functions (i.e., their positions would be precisely

All authors are with Harvard University, Cambridge, Massachusetts 02138; C. Papaliolios is in the Harvard-Smithsonian Center for Astrophysics and Department of Physics; P. Nisenson is in the Harvard-Smithsonian Center for Astrophysics and Center for Earth & Planetary Physics; and S. Ebstein is in the Division of Applied Sciences.

Received 9 August 1984.
0003-6935/85/020287-06$02.00/0.

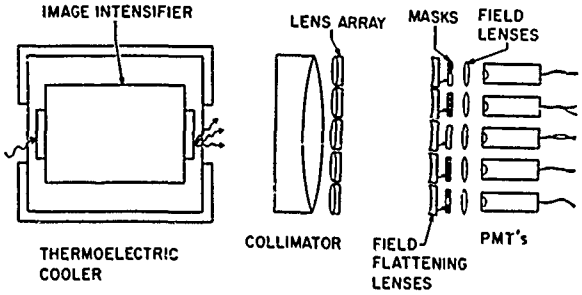

Fig. 1. Diagram of the PAPA two-dimensional photon detector.

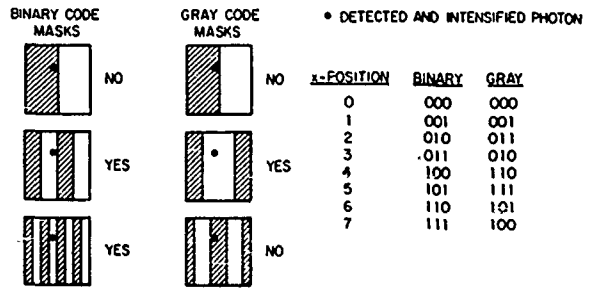

Fig. 2. Principle of Gray-coded masks for photon position detection.

specified, to the resolution of the camera) and would preserve the timing information down to ~1 msec. In this case the photon noise bias associated with the quantized signal could be completely removed.[2] In addition, the ability to easily transfer this information into a computer would be very important. At low count rates, several existing cameras could be used, such as a video system with digital centroiding. However, the camera we required would have to function at least at a rate of 100,000/sec.

III. Principle of Operation

Each photon detected at the photocathode of a high-gain image intensifier produces a bright spot at the output face of the intensifier. The measurement of the spot position consists of a series of binary decisions. A photomultiplier looking at an image of the intensifier output face determines that a photon has been detected somewhere in the field. Another phototube looking at an identical image but through a mask that is clear on the left half and opaque elsewhere determines whether the detected photon is in the left half of the field if it sees it or in the right half if it does not. Each succeeding phototube, looking through an appropriate mask at its image of the intensifier, determines one more bit in the x or y address of the photon. In this way nine phototubes determine the position in the x direction to one of 512 locations and nine more phototubes similarly determine the y position. The resulting 18-bit x-y address is recorded on tape for later entry into a computer. The sequence of addresses thus generated is recorded in the same order as the arrival times of the photons.

IV. Description of the Camera

The optical layout of the camera is shown in Fig. 1. A photon detected at the photocathode of the high-gain image intensifier produces a bright spot at the intensifier output. The light from this spot is collimated by the large lens and an array of identical small lenses, each picking off a small bundle of collimated light, forms multiple images in its focal plane. The $f/2.8$ Kodak Aero-Ektar lens and the array of achromtic doublets are of sufficient optical quality to accurately image the 40-μm spot at the output face of the intensifier onto the masks. The image formed by each small lens is a copy of the output face of the intensifier. A mask is placed in each of these image planes, except for one which we call the strobe channel. To uniformly illuminate the phototube, a field lens immediately follows each mask.

The masks used in the camera are Gray-coded rather than binary-coded. Gray code has the property that only 1 bit changes in the digital address from one pixel to the next[1] (Fig. 2). Since only 1 bit of the Gray code changes between adjacent pixels, ambiguities associated with a photon crossing pixel boundaries can cause only a 1-pixel error in the decoded position. The contrast with a binary coded system is dramatic. A photon crossing the center of the field causes a change in all binary bits. If the bits do not switch simultaneously, the decoded position can yield an address that is anywhere in the field.

V. Photon Camera Electronics

For each detected photon event, the pulse outputs from the photomultipliers are integrated by fast, gated integrators. Since the intensifier has a finite spot size (although smaller than 1 pixel in diameter), a threshold for deciding whether a photon has landed in the clear or opaque area of a mask must be set. First, a threshold is set in the strobe channel below which pulses approach system noise levels (typically this is 30–40% of the mean pulse height). Then all other thresholds are dynamically set to half of the strobe channel pulse height. This comparison is valid for pulses of a wide range of amplitudes, so that only the smallest pulses from the intensifier's exponential pulse height distribution are excluded.[6] The result of all the comparisons is the digital x-y position for the event.

After each event is detected, the address of the photon is latched and the integrators are reset. The stream of addresses, converted digitally from a gray to a binary code, is encoded on a video carrier and recorded serially onto a videocassette tape. The binary address is also D–A converted to provide a real-time display on an x-y scope. In addition, a microcomputer samples the data stream, allowing for some processing and image integration at the telescope. Back in the laboratory, the data are stripped from the video tape onto computer magnetic tape, allowing digital processing at the integrating computer.

VI. Basic Laboratory Tests

Figure 3 contains two direct integrated images recorded with the PAPA detector. Each was recorded at a count rate of 60,000 counts/sec and contains ~3.6 million detected photons. While the camera does have

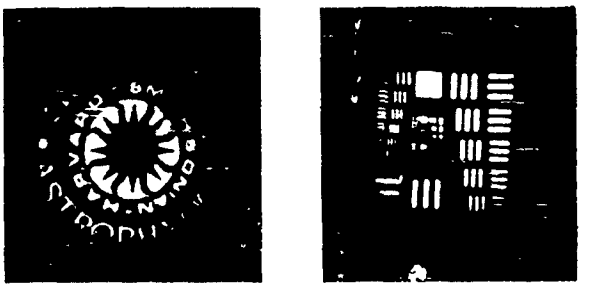

a. b.

Fig. 3. Direct images recorded with the PAPA detector at a data rate of 50,000 counts/sec.

512 × 512 pixels, the current data recording technique is limited to the most significant 8 × 8 bits (256 × 256 pixels). Using the 8 least significant bits in the x and y photon addresses, we have imaged test targets which demonstrate resolution at the 512 × 512 scale. At the scale normally used (256 × 256 pixels), integrated images of flat fields (uniformly illuminated fields) indicate pixel-to-pixel variations of ~30% rms. These nonstatistical variations, which are presumed to be due to mask misalignments and imperfect optics, seem to be stable and are eliminated by standard flat-fielding operations in the computer. The flat-fielding operation, important when the camera is used to produce accurate integrated images, is relatively unimportant for speckle applications since the artifacts fall almost entirely along the axes in frequency space. However, since the flat-field correction is done so easily in an array processor, we routinely perform it on all the data acquired.

VII. Speckle Results

The PAPA camera has now been used on three speckle observing runs on three different telescopes: the Steward Observatory 229 cm (90 in.) on Kitt Peak, the Smithsonian Astrophysical Observatory–University of Arizona Multiple Mirror Telescope, and the University of Hawaii 224 cm (88 in.). On each run the camera worked without any problems and produced many usable data sets of technical and scientific value. We demonstrate the quality of the results with a few examples from the first data obtained with PAPA on the Steward 229 cm speckle run in November 1983.

Figure 4 shows a long exposure, a reconstruction, a power spectrum, and a representation of the transform phase (reconstructed using the Knox-Thompson phase recovery algorithm[4]) for a 0.5-arcsec separation binary SAO 93840. In the phase image, black corresponds to −180° and white to +180°. The two components are magnitude 8 and 9, and the recording data rate was 40,000 photons/sec. This star was not known as a double prior to this run. Figure 5 shows a direct integration of a data set on the same star for various exposure times. Figures 6 and 7 demonstrate the effect of the frame time (relative to the atmospheric correlation time) on the reconstructed power spectra and images, respectively. The time-ordered photon list recorded with the PAPA allows partitioning the data in arbitrary time bins. The data were processed for equal signal-to-noise, i.e., the number of frames varied inversely as

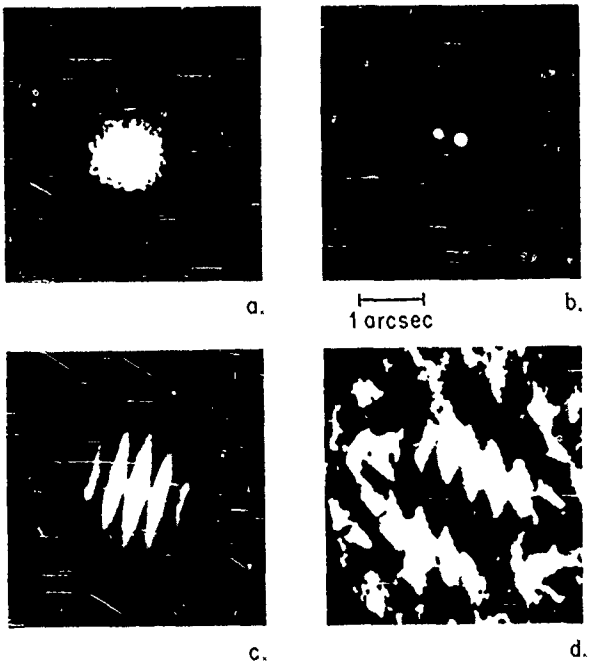

a. b. c. d.

Fig. 4. Reconstruction of SAO 93840 using 6000 frames at 60,000 counts/sec. (a) direct sum, (b) image, (c) power spectrum, (d) recovered transform phase.

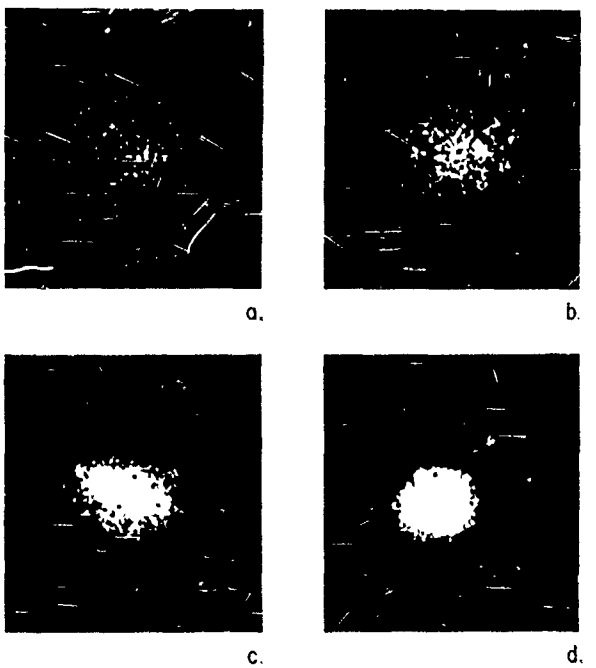

a. b. c. d.

Fig. 5. Direct images of SAO 93840 for different integration times. (a) 0.001 sec, (b) 0.01 sec, (c) 0.1 sec, (d) 100 sec.

the square of the number of photons per frame. It is surprising that even for frame times as long as 360 msec there is still substantial correlation at low angular frequencies. Figures 8 and 9 show the influence of the length of the integration on the quality of the recovered power spectra and images.

Figure 10 contains the image, autocorrelation, and power spectra for Delta Ori, a bright star with a faint companion (3 magnitudes difference). Figure 11 shows another star, Gamma Ori, with a previously undetected

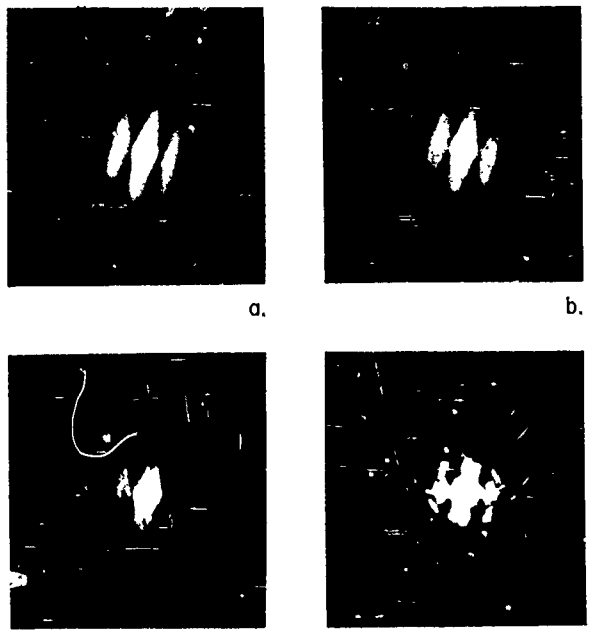

Fig. 6. Effect of frame (exposure) time on the power spectrum for SAO 93840: (a) 20 msec, (b) 80 msec, (c) 180 msec, (d) 360 msec.

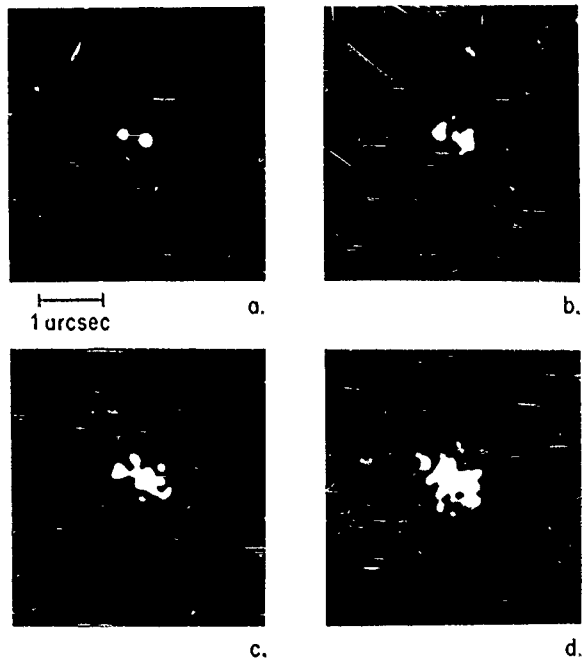

Fig. 7. Effect of frame (exposure) time on the reconstructed image for SAO 93840: (a) 20 msec, (b) 80 msec, (c) 180 msec, (d) 360 msec.

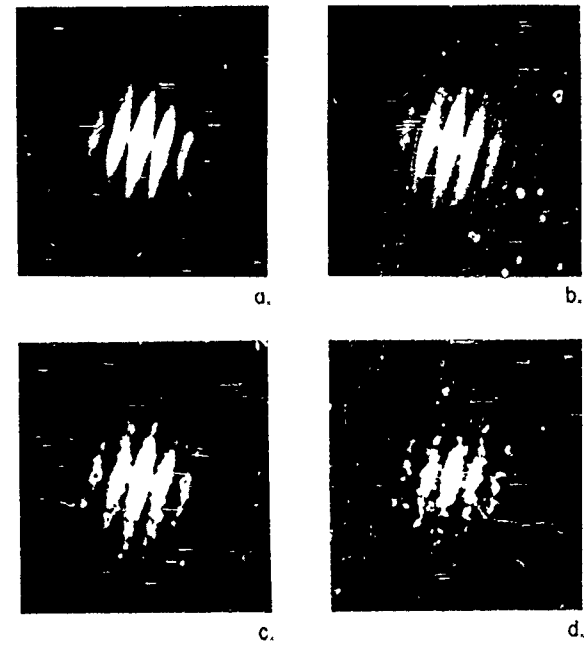

Fig. 8. Convergence of the power spectrum for SAO 93840 as a function of number of frames. (a) 6000, (b) 1600, (c) 400, (d) 100.

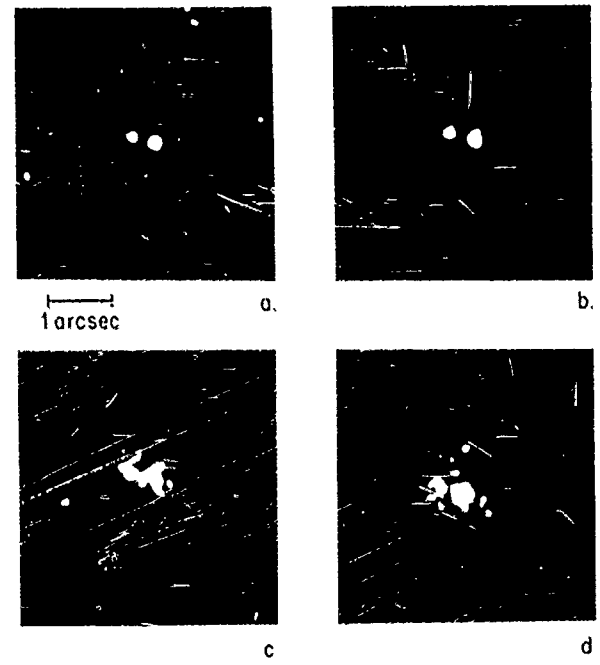

Fig. 9. Convergence of the reconstructed image for SAO 93840 as a function of number of frames. (a) 6000, (b) 1600, (c) 400, (d) 100.

companion. The two components have a magnitude difference of 5 with separation of 0.8 arcsec. Because of the brightness of both Delta and Gamma Ori, a neutral density filter of 0.9% had to be used to reduce the signals to a level within range of our data recording capabilities. Delta Ori was recorded at a data rate of 22,000 photons/sec and Gamma Ori at a data rate of 40,000 photons/sec. Figure 12 shows the image, autocorrelation, and power spectrum for Vesta, a 0.3-arcsec diam asteroid. Here the data rate was 60,000 photons/sec. All three integrations were performed using a frame time of 20 msec and ~12,000 frames (4 min of data). While this is only a small sample of the data recorded and processed, the results demonstrate the linearity and dynamic range of the camera and its potential for speckle data recording.

VIII. Camera Properties

The PAPA detector, made from easily available off-the-shelf parts, is a 2 D photon camera that provides a time-ordered list of photon positions. Currently, it can handle count rates of at least 200,000/sec and it provides 512 × 512 pixel resolution.

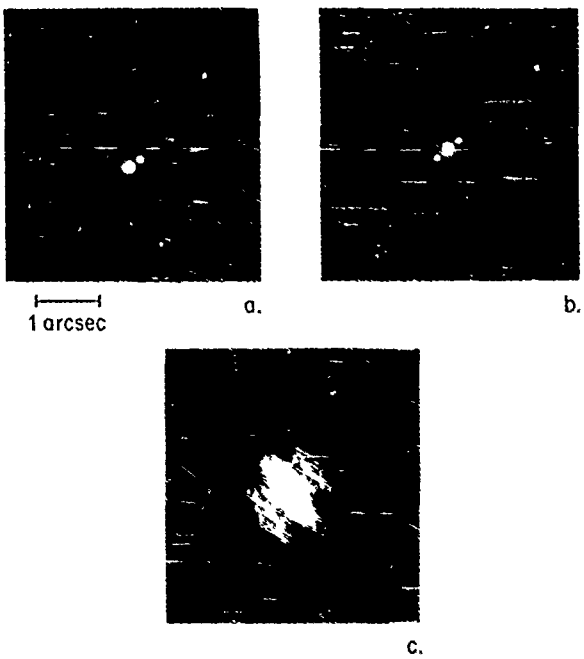

Fig. 10. Delta Orionis and its companion. Binary separation = 0.3 sec of arc, V (magnitude difference) = 3. (a) image, (b) autocorrelation, (c) power spectrum.

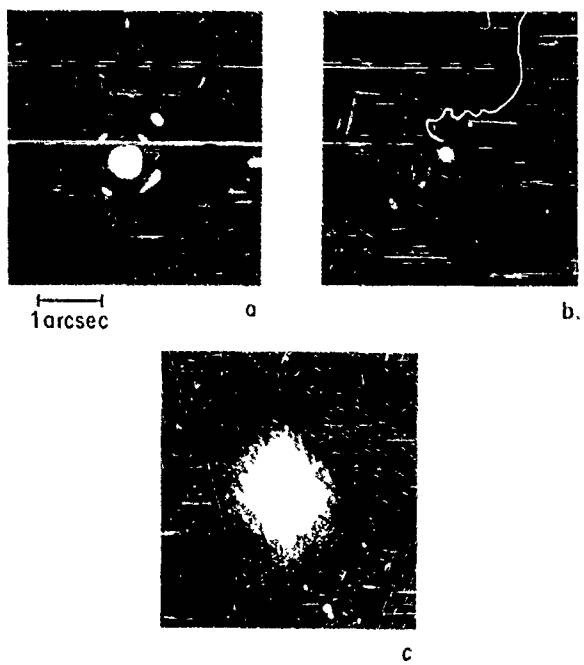

Fig. 11. Gamma Orionis and its companion. Binary separation = 0.8 sec of arc, V (magnitude difference) = 5: (a) image, (b) autocorrelation, (c) power spectrum.

The spatial resolution can certainly be increased by going to a larger diameter intensifier (the present version uses a 25-mm diam tube) or by using interpolation of the measured pulse height in each channel to obtain the extra bits of resolution. Unlike the resistive anode type of detectors which use centroiding and interpolation to provide the entire address information, most of the address information would still be provided by the masks and only the last few bits would come from the interpolation procedure. We believe it is possible to

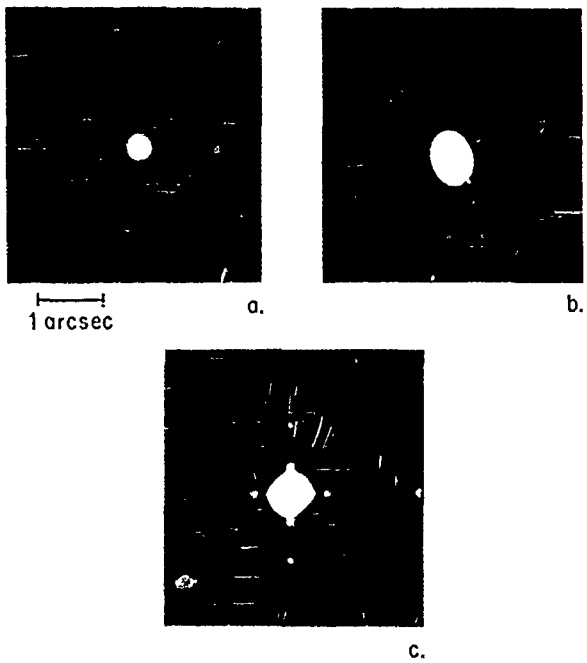

Fig. 12. Reconstruction of the resolved (0.3 sec of arc) asteroid Vesta (data rate of 70,000 counts/sec). (a) image, (b) autocorrelation, (c) power spectrum.

build a camera with up to 4000 × 4000 pixel resolution and requiring only a modification of the analog electronics. The details of the interpolation will be discussed in a subsequent paper.

The maximum count rate can also be increased somewhat just by improving the pulse electronics that follow the phototubes. The phosphor rise time of 20 nsec and decay time of 200 nsec, measured for the *P*-47 phosphor that is used on our intensifier, should allow the construction of a camera that could handle 1,000,000 counts/sec and lose only ~20% of the photons due to overlap.

The present version of the camera uses a single Generation II microchannel plate intensifier with an extended-red *S*-20 photocathode which has a peak quantum efficiency of 4%. The camera electronics are set at a level in which three-quarters of the pulses are accepted, so the actual detector efficiency is 3%. We plan to couple a diode intensifier to the front of the microchannel plate tube to increase the overall quantum efficiency to an expected 15%. The one potential problem with a two-intensifier system is the increased geometric distortion in the conventional electron optics. However, this distortion can be corrected with a field lens located near the input face of the first intensifier, which introduces an inverse distortion compensating for the measured intensifier characteristic.

There are many applications for which this camera is of obvious value. It provides data in a convenient format for computer processing and the data rate is set by the number of photons detected, not by the number of resolvable pixels. The arrival time of the detected photons is preserved and can be recorded to a precision of under a microsecond. In addition to the speckle applications already discussed, it could serve as the

camera for a high spectral resolution echelle spectrometer with crossed dispersion, as has been suggested,[1] or as a star guider or tracker in a sparse field of faint stars.

IX. Discussion

A new camera has been built to record the x-y positions of individually detected photons. It appears to approach the ideal low light level camera for our speckle work and preliminary data taken on three recent observing runs confirm this. For the first time we can make the essential photon noise bias correction that is always required for analysis of low light speckle data. This camera has opened up a new field that we plan to exploit.

We wish to acknowledge the many useful discussions and supportive interest of Lawrence Mertz, Richard Goody, Robert Stachnik, Robert Noyes, and Keith Hege. We also wish to thank Joseph Lehar for help in the data reduction, Louis DeFeo for aid in the camera construction, and Richard Cromwell for help in measuring the camera quantum efficiency. This work was partially supported by grant NGL-22-007-228 of the National Aeronautics and Space Administration and by grant AFOSR-81-0055 from the Air Force Office of Scientific Research. It gives us great pleasure to thank William Brunk (NASA) and Henry Radoski (AFOSR) who have been extremely supportive throughout the development of this detector.

References

1. C. Papaliolios and L. Mertz, "New Two-Dimensional Photon Camera," Proc. Soc. Photo-Opt. Instrum. Eng. **331**, 360 (1982).
2. P. Nisenson and C. Papaliolios, "Effects of Photon Noise on Speckle Image Reconstruction with the Knox-Thompson Algorithm," Opt. Commun. **47**, 91 (1983).
3. A. Labeyrie, "Attainment of Diffraction Limited Resolution in Large Telescopes by Fourier Analysing Speckle Patterns in Star Images," Astron. Astrophys. **6**, 85 (1970).
4. K. T. Knox and B. J. Thompson, "Recovery of Images from Atmospherically Degraded Short-Exposure Photographs," Astrophys. J. **193**, L45 (1974).
5. P. Nisenson, J. Apt, R. Goody, and C. Papaliolios, "Speckle Imaging for Planetary Research," Icarus **53**, 465 (1983).
6. T. Gonsiorowski, "Variable Threshold Discrimination in a Photon-Imaging Detector," Appl. Opt. **23**, 1060 (1984).

APPENDIX
B

Digital recording on video cassette

Steven Ebstein

Division of Applied Sciences, Harvard University, Cambridge, Massachusetts 02138

(Received 25 October 1982; accepted for publication 29 March 1983)

A system is described that records digital data onto video cassettes and writes the data to a computer tape for subsequent processing. The system is capable of recording and playing back 172 800 bytes/s. This corresponds to the maximum rate achievable with a nine-track computer tape drive writing 1600 bits per inch at 125 ips. A standard two-hour cassette has a capacity of 1.2 Gbytes. Six checkbits are written with each 16-bit word to facilitate error detection and correction. Upon playback, the data are written via DMA into a computer and then to a nine-track computer tape. Error rates of less than 1 word in 300 000 have been achieved with an off-the-shelf portable video recorder and commercially available tape. The system comprises a low-cost solution to the problem of high-volume, fast data recording at remote locations when a small error rate can be tolerated.

PACS numbers: 06.50.Dc

INTRODUCTION

Video cassettes are capable of extremely rapid and dense information storage with a small error rate upon recovery. Thus, they have been used as a recording medium for Winchester disk backup systems.[1] Given the portability of the recorders, the video cassette is an excellent means of recording large amounts of data at remote sites where it is inconvenient to set up larger and less rugged computer tape drives and their processors. When one adds the fact that video cassette recorders (VCR's) are inexpensive, one can see why some astronomers have begun to adopt the video cassette as a digital data recording medium.[2]

A system for recording digital data onto video cassette was constructed for use with a new photon camera.[3] The camera yields a 16-bit position for each detected photon. Due to the stochastic nature of the data arrival times, an asynchronous system was developed. The system has also been used to record data from a CCD camera.

The system, shown schematically in Fig. 1(a), has four parts—a circuit to encode the digital data in a video format, a modified portable VCR, a circuit to decode the data from the video signal upon playback, and a DMA interface to a computer which writes the computer tape.

I. ENCODER

The encoder circuit is comprised of a first-in, first-out (FIFO) memory to buffer the incoming data, an error-correction code generator, a parallel to serial converter, a video timing generator, and a circuit that combines the data and blanking signals into a standard video signal. A block diagram detailing the encoder is shown in Fig. 1(b). The encoder, like most of the circuitry in the system, consists of low-power Schottky (LS) TTL logic.

In order to understand the data flow, it is necessary to understand the format of a TV signal. The NTSC (National Television Standards Committee) standard for TV signals in the United States requires that the TV picture consist of 30 frames per second. Each frame consists of 525 horizontal lines. The frames are further split into two interlaced fields of 262.5 lines each. This method of presentation results in a flicker-free picture as perceived by the brain. Each line is scanned from left to right, and each field is scanned from top to bottom with some time allowed to retrace the position of

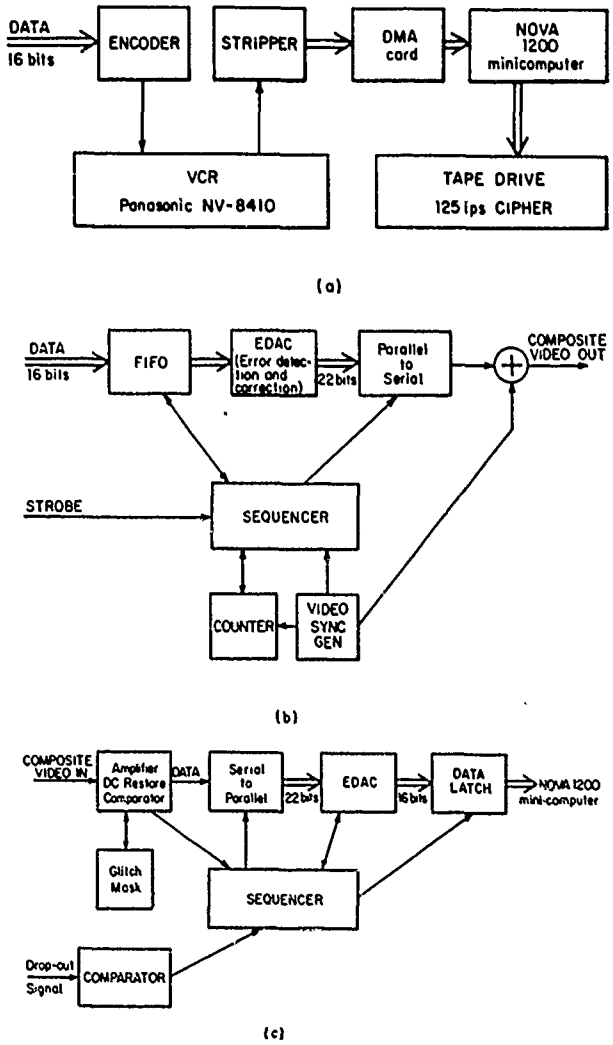

FIG. 1 (a) Block diagram of the overall videotape system; (b) block diagram of encoder (recording); (c) block diagram of stripper (playback).

 0034-6748/83/070883-03$01.30

the electron beam at the beginning of each line and each field. Thus, each horizontal line starts with a horizontal blanking pulse during which no information can be conveyed. Similarly, each field begins with a vertical blanking pulse. If we denote the duration of each horizontal line by H, the blanking pulses last $0.17H$ and $21H$, respectively.

During these blanking times, which occupy approximately 25% of the total time, no data can be written to the recorder. A FIFO memory is used to buffer the data during the various blanking times. To minimize the dead time during which the encoder cannot accept data, a fast 10-MHz 64×4 FIFO (Monolithic Memories 67401) is employed.

Error detection and correction (EDAC) is performed with a 74LS630, which takes a 16-bit data word and generates a 6-bit checkword via a modified Hamming code. Upon playback, the chip corrects all single-bit errors and flags all double-bit errors. To allow for unambiguous determination of the beginning of each new data word, start and stop bits, 1 and 0, respectively, are added to the 22-bit work comprised of data and checkword. Thus, each asynchronous word is 24 bits long. The data are output serially in a simple NRZ code.

The TV sync signal is generated by an MM 5321 (National Semiconductor) "sync generator" IC. The chip also provides horizontal and vertical blanking signals which are used to determine when a data word can be written. At the end of each horizontal blanking pulse, a pulse is triggered that defines the interval during which a data word can be written. The pulse length is adjusted so that a maximum of six words can be written on each line. In addition, only lines 23 through 262 are used for data, as lines 22 and 263 are half-lines every other field due to interlacing (lines 1 through 21 comprise the vertical blanking period).

When the signal indicating that a word can be written is true and a word is present at the FIFO output, the data are loaded into a serial shift register and clocked out. The clock is constructed by dividing a 56.6-MHz oscillator by 16. The clocked data signal is summed with the TV sync signal and the composite signal is then buffered for transmission over a 75-Ω cable. One field is shown in Fig. 2(a). A single horizontal line is depicted in Fig. 2(b).

II. RECORDER

The composite video signal is recorded with a portable VCR (Panasonic NV-8410) using half-inch tape recorded in "VHS" format. Three adjustments were made that are recorder dependent and are described as follows. We found that the signal recorded was both band limited and slew-rate limited. The band limiting was circumvented by adding a speedup capacitor in parallel with a low-pass filter that the recorder employs to reduce composite color signals to pure luminance signals (chrominance and luminance are encoded separately). The recorder appears to have frequency response much higher than the 3.6-MHz bit rate we employ. The slew-rate limit, however, limits recording to rates comparable with our bit rate.

The slew-rate limitation required our adjusting the relative amplitudes of the sync tips to the data such that the recorder could slew from the blanking level (logical zero) to full scale (logical one) in one bit period. The recording of a single data word is depicted in Fig. 2(c). As can be seen, the played-back signal just rises to full scale in one bit period. Some overshoot is present, but the data can be cleanly recovered in spite of the overshoot.

The last recorder-dependent adjustment involves head-switching transients. The recorder used has two revolving heads which are alternately in contact with the tape. A no-

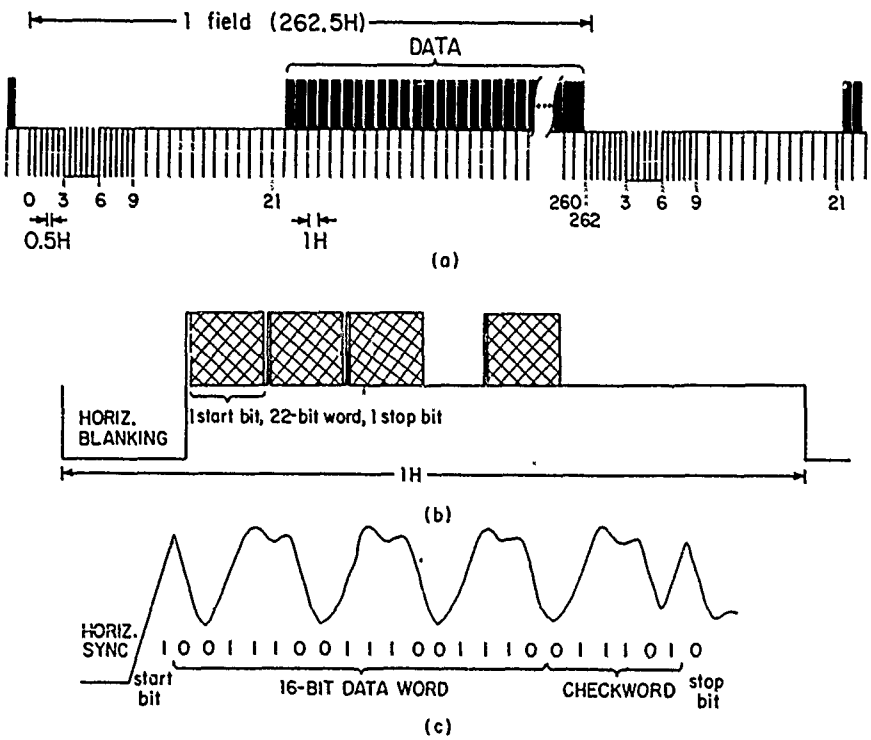

FIG. 2. (a) One video field; $H = 63.5\ \mu s$; (b) a horizontal line with input data rate less than the maximum; (c) recorder output of one word (playback).

ticeable glitch in the playback output occurs at the time when the switch takes place. It was necessary to adjust the phase of the recording such that the switch occurred during the vertical blanking interval. The glitch could then be easily masked out.

III. STRIPPER

The data are recovered upon playback by a simple level-detection scheme. The block diagram outlining the process is shown in Fig. 1(c). The video output of the recorder is first amplified, then dc restored, and a fast comparator with hysteresis is sufficient to obtain a clean copy of the input data. Upon detection of a start bit, the divide-by-16 clock is enabled and the data are clocked into a shift register. The resulting 22-bit word is presented to the error corrector. The error flags are examined and the (corrected) 16-bit data are latched in an output register. If two bits are in error, the word is discarded.

One feature of VCR's introduces a subtlety into the playback process. Dropouts of the FM-modulated signal on the tap frequently occur. These can result from imperfections in the recording medium or temporary loss of head-to-tape contact. With good-quality tape, they typically occur once every few seconds and last a few tens of microseconds.[4] To avoid the black or white streaks these dropouts produce, VCR manufacturers typically employ some form of dropout compensation. The Panasonic recorder delays the playback signal by 1*H*. When a dropout occurs, the output is switched to the delayed signal; i.e., it substitutes a portion of the previous horizontal line. Since TV pictures are very similar from line to line, this does not perceptibly degrade the playback image. For data recording, however, the result is catastrophic. For that reason, the dropout detector is monitored by the stripper. When a dropout occurs, the data are gated off until the beginning of the next horizontal line after the dropout ceases. This results in some data being thrown out. For the photon camera data, it does not matter if the list of photons recorded is shorter by less than one part in 10^5. For the CCD data, an encoding scheme is used which indicates when data words are dropped.

IV. DMA

In order to process the data, it is necessary to write a computer tape with the data, unless some special real-time processor is employed. We write computer tapes with a DMA interface to a 16-bit minicomputer (Data General Nova 1200). In order to keep data moving as fast as it can be written onto tape, double buffering is employed. The DMA interface and the program move data in and out of two equal-sized blocks. While the device is DMAing data into one block, the computer is DMAing the other block to tape. The program and device communicate via the Nova I0 device flags, Busy and Done.[5] This method is faster than using an equivalent interrupt-driven scheme.

Since VCR's take a few seconds to get up to speed and lock onto the synchronization pulses, the recorder is run continuously while data are being taken. Similarly, the data stream off the tape when it is played back and the tape drive and DMA channel must be fast enough to keep up. In practice, we limit the encoder to six words per line to ensure that the tape drive can write all the data. A 2400' 1600-bpi computer tape can hold just under 10 min of data recorded at the maximum rate.

V. DISCUSSION

The prototype of the system was wire wrapped by hand on four separate cards. We subsequently reproduced the encoder and stripper functions on a single card which was wire wrapped by machine. Additional copies of this card can thus be easily made; schematic diagrams of the circuitry are available upon request.

The system has been used to record data from a digital photon camera and a CCD camera. The CCD data have been recorded with the machine wire-wrapped implementation of the system. These data are a list of 12-bit intensities from successive pixels in the CCD array. A 3-bit counter and a beginning of line and frame bit are recorded with the intensity. These bits provide sufficient information to detect when a pixel has been dropped.

We find that the error rate is dominated by tape dropouts several tens of microseconds in duration, not by nonrecoverable double-bit errors occurring randomly in the data. The single- and double-bit error rates are observed to be less than or equal to the dropout rate, indicating that most of these errors are due to dropouts. With fresh tape we average 1 dropped word in 300 000 at the maximum data rate after error correction. This figure is meant to be representative and is liable to vary with tape quality. The dropped words tend to cluster; i.e., three or four successive words will be lost to one dropout.

The suitability of this recording technique for a given application depends on both the error tolerance and the redundancy employed in encoding the data. For instance, the nonrecoverable error rate could be reduced to 1 in 10^{11} by recording blocks of data twice and using software to restore blocks with dropped words. The commercial applications of digital recording on video cassette employ this sort of redundancy. For our purposes, it is sufficient to discard erroneous words and keep track of where these dropped words occur.

ACKNOWLEDGMENTS

I wish to thank Costas Papaliolios and Paul Horowitz for their suggestions and Pete Nisenson for his assistance. The automated wire wrap was programmed with a CAD/CAM system written by Kok Chen at Stanford University. The support of NASA Grant No. NGL-22-007-228 and an NSF graduate fellowship are gratefully acknowledged.

[1] Corvus Systems, Inc., 2029 O'Toole Ave., San Jose, CA 95131; Alpha Microsystems, 17881 Sky Park North, P. O. Box 18347, Irvine, CA 92713.
[2] L. Mertz, T. D. Tarbell, and A. Title, Appl. Opt. 21, 628 (1982).
[3] C. Papaliolios and L. Mertz, in *Instrumentation in Astronomy IV*, edited by D. L. Crawford, SPIE Proceedings (Society of Photo-Optical Instrumentation Engineers, Bellingham, WA), Vol. 331, pp. 360–364.
[4] Norm Ritter, 3M Co., Minnesota (private communication).
[5] *How to Use The Nova Computers*, Data General Corp., Southboro, MA

APPENDIX
C

Constrained Iterative Deconvolution of Noisy 2-D Images

Steven Ebstein
Division of Applied Sciences
Harvard University
Cambridge, MA 02138

A constrained iterative technique is demonstrated which deconvolves appropriately prefiltered noisy images. Convergence measures and performance with imperfect data are discussed.

Constrained Iterative Deconvolution of Noisy 2-D Images

Steven Ebstein
Division of Applied Sciences
Harvard University
Cambridge, MA 02138

Introduction

Constrained iterative restoration algorithms have been extensively studied [eg. 1-3]. They have been widely applied to the one-dimensional deconvolution problem [4]. Our purpose is to demonstrate that noisy two-dimensional images can be deconvolved by these techniques. We address the practical problems that arise and demonstrate that the technique yields reasonable images in the presence of noise and imperfect data.

Algorithm

We seek the object x that satisfies the functional equation

$$y = Dx \tag{1}$$

where D, the distortion operator, represents convolution with a point-spread function (PSF) and y is the blurred image we detect. The iteration is then given by

$$x_{k+1} = Cx_k + \alpha(y - DCx_k) \tag{2}$$

where C is a constraint operator and α is the relaxation parameter. The constraint operator enforces the positivity of the object and sets it to zero outside some region of support. The first guess, x_0 is set equal to αy.

Schafer et al discuss conditions for which this iteration converges and the optimal choice of α. The best choice for α is usually 2 when D has eigenvalues ≤ 1, though convergence is faster when α is allowed to vary [2].

When a noise term is added to the image, the iteration is not likely to converge. In particular, any high-frequency component to the image that is beyond the passband of the distortion cannot be reproduced.

Two internally derived error measures have been found which are observed to decrease monotonically when the iteration is converging. One is:

$$E_1 = \frac{\sum |x[m,n]| \quad \text{for } m,n \text{ s.t. } x[m,n] \notin \text{constraints}}{\sum |x[m,n]| \quad \text{for } m,n \text{ s.t. } x[m,n] \in \text{constraints}} \tag{3}$$

ie. the ratio of the summed magnitude outside the constraints to the summed magnitude satisfying the constraints. The other is:

$$E_2 = \frac{\left| \sum x[m,n] - V_i \right|}{V_i} \quad \text{for } m,n \text{ s.t. } x[m,n] \in \text{constraints} \qquad (4)$$

where $V_i = \sum y[m,n]$, ie. V_i is the integral (volume) of the image.

Clearly, the solution must have the same volume as the blurred image because convolution preserves the volume of positive objects. Internally derived error measures are essential for determining that the iteration is converging when the data are noisy and the PSF imperfectly known.

Results

We implemented the iteration in equation 2 on an array processor with image and object discretized to a 128x128 grid. The convolution is done by multiplication of discrete Fourier transforms (circular convolution). Each iteration costs two FFT's (of the object only) and takes ~1.2s with a 5 Mflop array processor. Adequate computing power is important with this algorithm because it converges slowly [1].

Two test objects were generated, an impulsive and an extended object. The impulsive object was a pair of delta functions 10 pixels apart and the extended object was a Gaussian with FWHM 16 pixels. The objects were convolved with a Gaussian . F with FWHM 16 (ie. the extended object) to generate the blurred images. Then, a photon-noisy image was generated by taking a Poisson pseudo-random deviate corresponding to the intensity at each pixel in the image. The intensity was scaled so that the brightest pixel in the image had a photocount of 200. The objects and their blurred and photon-noisy images are pictured in Fig. 1.

When the noiseless images were deconvolved with perfect PSF's, the output approached an exact copy of the input. The extended object took ~50 iterations to converge. The double had not converged after 30000 iterations, though the iterates were stably approaching the original object. The iteration essentially continues the Fourier transform out to higher frequencies. The number of iterations required depends on the degree of high frequency enhancement which is needed.

When the photon noisy images were used as input, the iteration diverged, as measured by E_1 and E_2. The iteration produced a set of points which bore no resemblance to the object. Following the suggestion of Schafer et al [1], we tried filtering the input image to reduce spurious high frequencies.

The first approach we tried was to low-pass filter the noisy image, eliminating all frequencies beyond the 70dB passband of the PSF. The iterates generated had increasingly higher

resolution and structure that resembled the original object with some artifacts. However, E_1 and E_2 were increasing indicating that the iteration would not converge to the correct object.

The next approach was to convolve the noisy image with the original PSF. This reblurred image and a similarly reblurred PSF were used as inputs to the iteration. E_1 and E_2 now decreased with successive iterates. The iterates no longer had artifacts and stably converged on the original object. The deconvolutions of the double and extended object are pictured in Fig. 2. The extended object converged after 200 iterations; the iteration was still converging on the double after 31000 iterations but had already achieved significant resolution enhancement.

We tried deconvolving with a noisy PSF and a perfect image. The iteration again converged if the inputs were prefiltered by blurring with the PSF. Unlike blind deconvolution (division of Fourier transforms), constrained iterative deconvolution does not require perfect knowledge of the PSF since errors in the object and PSF contribute equally to errors in the next iterate.

We tried deconvolving with the wrong PSF, a Gaussian that was twice as wide or twice as narrow than the correct PSF. When a narrower PSF was used, the iteration converged to an blurred version of the original object with some artifacts. The degree of blurring and artifacts depends on the mismatch of the PSF. This object, when convolved with the narrow PSF, reproduces the image. When a wider PSF was used, the iteration diverged, though it generated objects whose structure resembled that of the true object.

Conclusion

We have demonstrated that blurred, photon noisy images can be deconvolved with an iterative technique. The degree of resolution enhancement depends on the noise in the data and the computing power one has available.

References

1. R.W. Schafer, R.M. Mersereau, and M.A. Richards, "Constrained Iterative Restoration Algorithms," Proc. IEEE 69, p. 432 (81).

2. J.L.C. Sanz and T.S. Huang, "Unified Hilbert space approach to iterative least-squares signal restoration," JOSA 73, p. 1455 (83).

3. V.T. Tom, "Constrained Iterative Signal Reconstruction Algorithms," Ph. D. Thesis, M.I.T. 1981.

4. P.A. Jansson, Deconvolution: with applications in spectroscopy, Academic Press, New York, 1984.

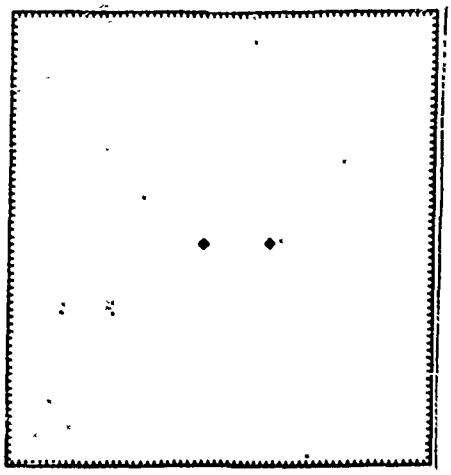

Fig. 1a Test double.

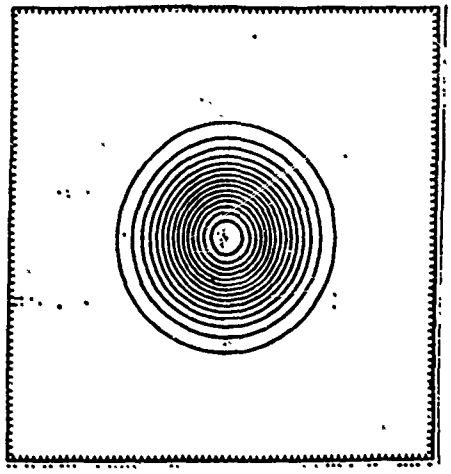

Fig. 1b Test extended object.

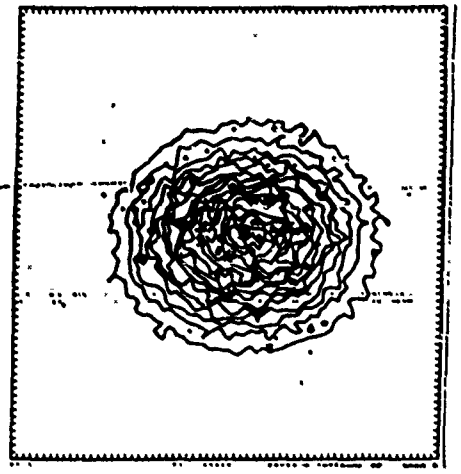

Fig. 1c Double convolved with PSF, photon noise.

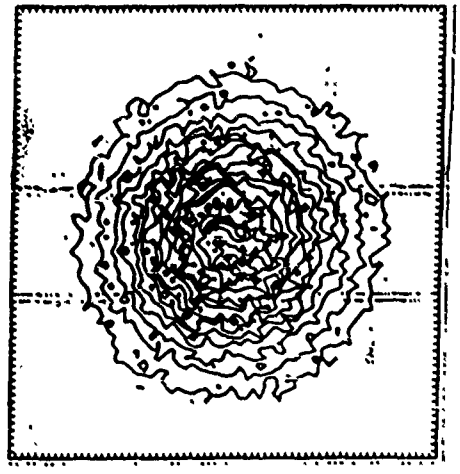

Fig. 1d Extended object convolved with PSF, photon noise.

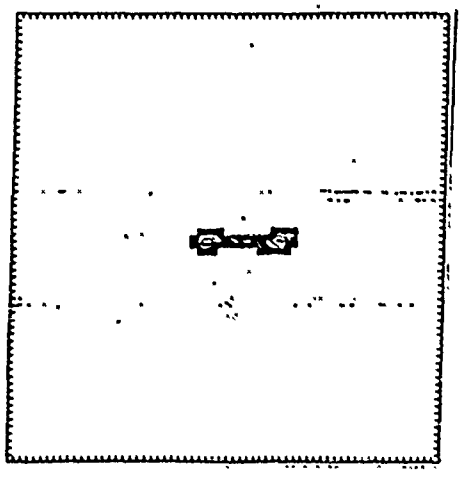

Fig. 1e Deconvolution of the double, 31000 iterations.

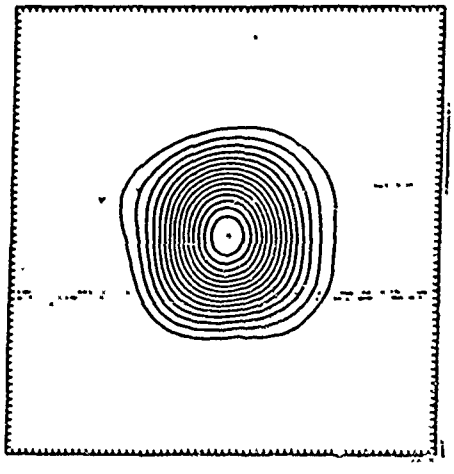

Fig. 1f Deconvolution of the extended object, 200 iterations.

APPENDIX
D

Signal-to-Noise in Photon Counting Speckle Interferometry with Real Detectors

Steven Ebstein
Division of Applied Sciences
Harvard University
Cambridge, MA 02138

The signal-to-noise ratio for speckle interferograms taken with the PAPA is compared to theory. Modifications for non-ideal detectors are discussed.

Signal-to-Noise in Photon Counting Speckle Interferometry with Real Detectors

Steven Ebstein
Division of Applied Sciences
Harvard University
Cambridge, MA 02138

Introduction

In speckle interferometry, one estimates the angular power spectrum of short-exposure images degraded by atmospheric turbulence. The power spectrum is a random process due to the variability of atmospheric conditions and due to the stochastic nature of photodetection. Considering each image to be a sum of individually detected photons,

$$i(x) = \sum_j \delta(x - x_j) \tag{1}$$

where x_j is the coordinate of the jth photon, an unbiased power spectrum estimate (PSE) is [1]

$$P(u) = |I(u)|^2 - N \tag{2}$$

where N, the number of photons in the exposure, is the photon-noise bias.

The signal-to-noise ratio (SNR) of the PSE has been studied by many authors [1-6]. For the estimator in equation 2, the SNR for each short-exposure PSE, defined as the power divided by the square root of its variance, is [1]

$$SNR = \frac{\bar{N}\,\hat{\phi}(u)}{((1 + \bar{N}\,\hat{\phi}(u))^2 + \hat{\phi}(2u))^{1/2}} \tag{3}$$

where $\hat{\phi}(u) = P(u)/P(0)$ and $\bar{N}$ is the mean number of photons per exposure. The derivation is valid for angular frequencies beyond the seeing cutoff where the PSE tends to a circular complex Gaussian random process. The term at 2u is never significant since $\bar{N}\,\hat{\phi}(u) \gg \hat{\phi}(2u)$ for all practical cases. The SNR equals one in the high-light-level case (atmospheric noise only) and is proportional to $\bar{N}$ for the low-light-level case. The transition occurs for $\bar{N}\,\hat{\phi}(u) = 1$. We note that for a point source, $\bar{N}\,\hat{\phi}(u)$ is the order of the number of photons per speckle [1].

Experimental Data

We have investigated the validity of equation 3 for speckle data

taken with the PAPA detector [7,8]. Speckle data were obtained in the laboratory for a point source with a rotating ground glass simulating the turbulent atmosphere. In addition, data taken with the Steward Observatory 90" telescope on Kitt Peak of a star, SAO 94927, were examined.

The data, in the form of a time-ordered list of photon addresses, were divided into a sequence of frames. Each frame consists of a fixed number of photons corresponding to the photon rate and the frame time. Each frame generates an image using equation 1 discretized on a 128x128 grid. The PSE for each frame was calculated using a discrete Fourier transform and averaged. The logarithm of the average PSE is shown in Fig. 1 for both data sets. Then, the variance of the PSE for each frame was estimated using the average PSE as the mean value. The observed SNR was compared to equation 3 along the line u=11 to avoid the artifacts along the axes.

The ratio of theory to observed SNR is plotted in Figs. 2 and 3 for a wide range of frame times and photon rates. These data span a range of $\bar{N}\,\hat{\Phi}(u)$ from .0004 to 20 and the data match the theory to within 10 %. The predicted SNR exceeds the observed SNR at low frequencies for the Steward data, possibly because the atmospheric statistics were not stationary.

Extension to non-ideal detectors

Equations 1-3 describe the situation for an ideal detector. A real detector will generally have a non-uniform sensitivity. For example, the present version of the PAPA has pixel size variations due to mask misalignment that lead to striping in the image and artifacts along the axes in the power spectrum. The image is then better represented as

$$I'(x) = \sum_j f(x_j)\,\delta(x - x_j) \qquad (4)$$

where f is a weight that flattens the field. Calculating the Fourier transform of i' in the standard fashion [3] leads to the unbiased PSE:

$$P'(u) = |I'(u)|^2 - N\,\overline{f^2} \qquad (5)$$

where $\overline{f^2}$ is the mean-square weight of a photon.

The flat-fielded images give power spectra with much reduced axial artifacts as is seen in Fig. 1. Detailed but straightforward calculation of the variance of P' [1,2,5,6] yields the SNR for flat-fielded images:

$$SNR = \frac{\bar{N}\,\hat{\Phi}(u)}{\left((\overline{f^2} + \bar{N}\,\hat{\Phi}(u))^2 + \hat{\Phi}(2u) \right)^{1/2}} \qquad (6)$$

This is identical to equation 3 in the high-light-level case but there is additional photon noise due to the non-uniform gain.

The photon-noise bias and SNR for the Knox-Thompson process are modified in a similar fashion. The unbiased estimator for the Knox-Thompson cross-product [6] becomes

$$P'_u(u) = I'(u)^* I'(u+du) - G(du) \tag{7}$$

where $G(\cdot)$ is the Fourier transform of

$$g(x) = \sum_j f^2(x_j)\delta(x - x_j) \tag{8}$$

Conclusion

We have verified the SNR expression for speckle interferometry and described the modification when a detector with non-uniform gain is used.

References

1. J.C. Dainty and A.H. Greenaway, "Estimation of spatial power spectra in speckle interferometry,", JOSA 69, p. 786 (79).

2. F. Roddier, "Signal-to-noise ratio in speckle interferometry," in Imaging in Astronomy, AAS/SAO/OSA/SPIE Topical Meeting, preprints paper ThC6, Boston (75) unpublished.

3. J.W. Goodman and J.F. Belsher, "Fundamental limitations in linear invariant restoration of atmospherically degraded images," SPIE Proc. 75, p. 141 (76).

4. M.G. Miller, "Noise considerations in stellar speckle interferometry," JOSA 67, p. 1176 (77).

5. A.H. Greenaway and J.C. Dainty, "The formal equivalence between autocorrelation and power spectral analyses of photon-limited data," Opt. Comm. 35, p. 307 (80).

6. P. Nisenson and C. Papaliolios, "Effects of photon noise on speckle image reconstruction with the Knox-Thompson algorithm," Opt. Comm. 47, p. 91 (83).

7. C. Papaliolios and L. Mertz, "New two-dimensional photon camera," Proc. SPIE 331, p. 360 (82).

8. C. Papaliolios, P. Nisenson, and S. Ebstein, "Speckle imaging with the PAPA detector," Appl. Opt. 24, p. 287 (85).

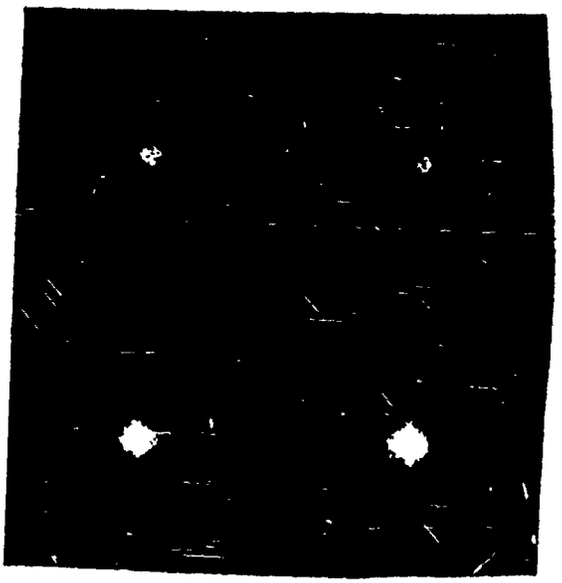

Fig. 1 clockwise from top left: log power spectrum of lab data, flat-fielded, SAO 94927 flat-fielded, not flat-fielded.

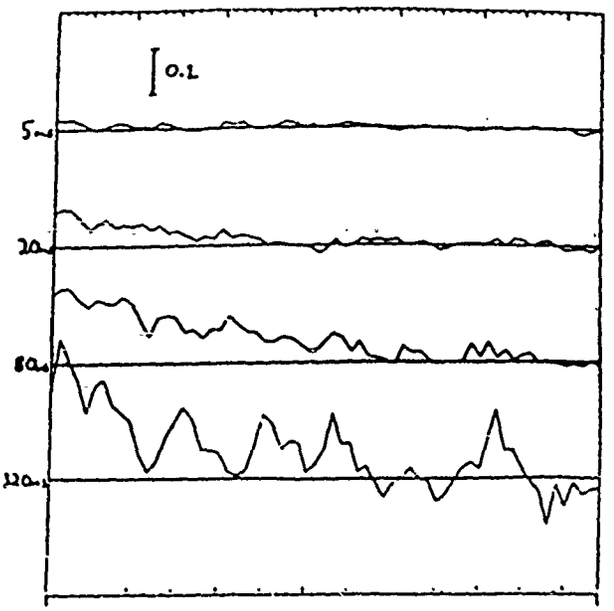

Fig. 2 Ratio theory/observed SNR SAO 94927, 67kHz photon rate, frame times in ms, 4 min. of data, line = 1.0.

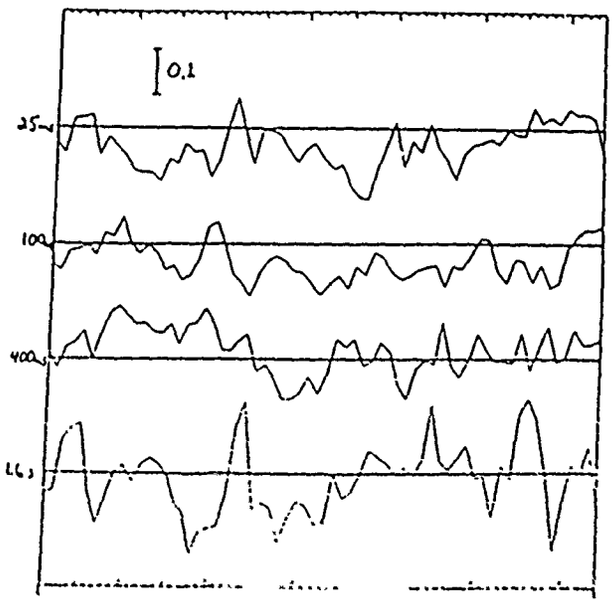

Fig. 3a Ratio theory/observed SNR lab data, 70kHz photon rate, frame times in ms, 4 min. of data, line = 1.0.

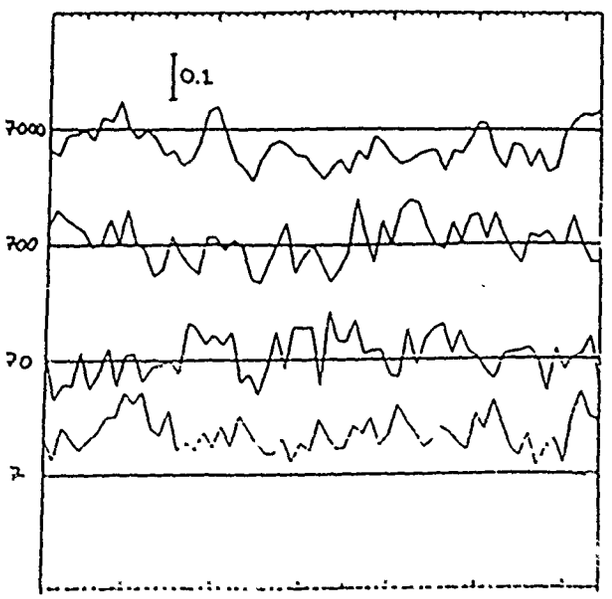

Fig. 3b Ratio theory/observed SNR lab data, 1000 frames, 7, 70, 700, 7000 photons/frame, line = 1.0.

APPENDIX

E

THE ASTROPHYSICAL JOURNAL, 297:L17–L20, 1985 October 1

A NEW OPTICAL SOURCE ASSOCIATED WITH T TAURI

P. NISENSON, R. V. STACHNIK, M. KAROVSKA, AND R. NOYES
Harvard-Smithsonian Center for Astrophysics
Received 1985 June 4; accepted 1985 July 5

ABSTRACT

A faint optical source close to T Tauri has been detected using speckle imaging techniques in a photon-counting mode of operation. This second optical source is located at position angle 358° ± 5° with a separation of 0".27 ± 0".04 from the optical astrometric position of T Tauri. The visual magnitude difference with respect to the primary, measured at 521 nm, is $m_v = 4.33 \pm 0.09$. Speckle imaging techniques have produced true images which eliminate the 180° ambiguity normally associated with speckle interferometry, allowing the correct position of the source to be determined. Since the new source is located north of T Tauri, it is distinct from the radio/infrared object recently reported to be located 0".61 south of T Tauri. As expected from the predicted temperature of the southern component, the optical speckle observations did not detect the infrared source. If the new source is a stellar object, it appears to have a mass of between 0.2 and 0.35 $M_\odot$ and has a surface temperature of 3000 ± 200 K corresponding to spectral types M4–M8. This would be one of the lowest mass pre–main-sequence stars yet detected.

Subject headings: interferometry — stars: individual — stars: pre–main-sequence

I. INTRODUCTION

T Tauri is the well-known prototype for a class of emission-line variable stars associated with dark cloud complexes. As discussed by Rydgren, Strom, and Strom (1976), the properties defining the class are (1) irregular optical variability; (2) the presence of emission lines, both permitted and forbidden; (3) "veiling" of the spectrum by overlying continuous emission; (4) broad absorption lines suggesting rapid rotation; (5) P Cygni and inverse P Cygni emission-line profiles; and (6) infrared excesses. These objects are recognized as pre–main-sequence stars which have only recently formed from the dense cloud complexes with which they are associated.

T Tauri [$\alpha(1900) = 4^h16^m09^s$, $\delta(1900) = +19°17'54''$] has a K0 or K1 spectrum with an unusual history of variability: it is reported to have fluctuated irregularly between $m_v = +10$ and +14 until 1910, and has remained between +10 and +11 since that time (Lozinskii 1949). The star is located in the Taurus-Auriga cloud complex inside an emission nebula 20"–30" across which has the spectrum of a Herbig-Haro object (Schwartz 1975). Recent observations of T Tauri have found an infrared (Dyck, Simon, and Zuckerman 1982) and radio (Schwartz, Simon, and Howell 1984) source located 0".61 south of the optical position of T Tauri. It is fainter than T Tauri itself at all infrared wavelengths measured and has an estimated temperature of 800 K. However, at radio wavelengths from 1.3 to 20 cm it is much the stronger source. It has a spectral index of $\alpha < 0.7$ suggesting that the 6 cm flux is thermal emission from a warm, constant expansion velocity stellar wind (Schwartz, Simon, and Howell 1984). Emission at 6 cm is also seen at the optical astrometric position of T Tau. The faint infrared and bright radio sources south of T Tau are now assumed to coincide, despite some early confusion due to the 180° ambiguity in the infrared speckle interferometry data.

This *Letter* reports the discovery of a third component in the T Tauri system, a faint optical source located 0".27 north of the bright optical component. This source was discovered by using a new two-dimensional photon counting camera (Papaliolios, Nisenson, and Ebstein 1985) and the techniques of speckle imaging. Speckle imaging allows recovery of both the amplitude and phase in the Fourier transform of the recovered image so that a true image may be reconstructed. This image unambiguously demonstrates that the source is located to the north, on the opposite side of T Tau from the radio source.

II. OBSERVATIONS

Speckle observations of T Tauri at optical wavelengths were carried out on 1983 November 15 and 16 with the Steward Observatory 2.2 m telescope and on 1984 October 21 with the Mount Wilson observatory 2.5 m telescope. Both sets of observations were made using the Precision Analog Photon Address (PAPA) detector (Papaliolios, Nisenson, and Ebstein 1985), a two-dimensional photon counting sensor which records a catalog of sequential photon positions. This version of the PAPA has a maximum data recording rate of 100,000 photons s^{-1} in a field of 256 × 256 pixels. The photon addresses are encoded on a video carrier and stored using a conventional VCR for later digital processing. Speckle data recording uses a foreoptics package which provides (1) magnification of the image so that the diffraction-limited scale of the telescope is matched to the pixel size of the camera, (2) narrow-band filtering which yields temporal coherence sufficient for the optical path errors introduced by the atmospheric

aberrations, and (3) atmospheric dispersion correction with a prism compensator. An optics package developed by K. Hege of the Steward Observatory, University of Arizona was used for the run of the 2 2 m, and an equivalent system built at CfA was used for the Mount Wilson observations. The Steward observations were made with a 24 nm wide filter centered at 659 nm. At Mount Wilson, three different filters were used: a 74 nm wide filter centered at 673 nm, a 36 nm filter centered at 521 nm, and a 50 nm filter centered at 450 nm. Count rates ranged from 6000 photons s^{-1} in the red to 500 photons s^{-1} in the blue.

III. DATA PROCESSING

Digital processing of the recorded data involves conversion of the VCR format to standard digital tape storage using a buffered interface. The photon addresses are then divided into subsets with lengths matched to the characteristic correlation time of the atmosphere. This approach allows regrouping of the data for maximization of the signal-to-noise ratio in the integrated result. Typical correlation times range from a few to tens of milliseconds. Individual images are built from the photon list by incrementing the array position corresponding to a photon address. The Fourier transform for each image is calculated and accumulated into the complex correlation arrays required for speckle reconstruction (Nisenson and Papaliolios 1983). Compensation for the atmospheric and telescope transfer function is accomplished by the use of the data taken for an unresolved reference star, which is recorded close in time to the object data. This star is chosen to be as close in angular position to the object as possible so that the long-term atmospheric statistics are similar. Deconvolution by the reference star results in enhancement of the high angular frequencies in the reconstruction.

Until recently, compensation for the effects of photon noise on the reconstructed images has been difficult and inaccurate. However, the form in which the data is available from the PAPA detector, in which each photon's centroid and the total count is exactly known, allows precise compensation for the photon noise bias (Nisenson and Papaliolios 1983).

IV. RESULTS AND ANALYSIS

Processing of the data from the Steward 1983 November observing run revealed a previously undetected companion source to T Tauri in the visible. Low-contrast fringes in the power spectrum indicated the existence of a second source located in a north-south direction. An autocorrelation and an image were then reconstructed from the data set, and these revealed that the second source was located 0".27 ± 0".04 from the primary source, at a position angle of 358° ± 5°. Figure 1 (Plate L1) shows the recovered power spectrum, autocorrelation, and image from the T Tauri data. For comparison, the results from processing data for a binary star, SAO 93840, are shown. This data set was recorded a few minutes after the T Tauri observation, and this star was not known to be a binary until after processing. This binary has a separation of 0".38, a position angle of 10°, and the two stars are 8th and 9th mag, respectively. The apparent size of the star images in these figures is related to their relative brightnesses and not their angular size.

TABLE 1

MEASURED MAGNITUDE DIFFERENCES

Filter Width (nm)	Filter Center (nm)	Magnitude Difference	Telescope
74	673	3.53 ± 0.04	Mount Wilson 2.5 m
24	659	3.62 ± 0.05	Steward 2.2 m
36	521	4.33 ± 0.09	Mount Wilson 2.5 m
50	450	5.3 ± 0.2	Mount Wilson 2.5 m

NOTE.—Average separation (ρ) and position angle (θ) from four measurements: ρ = 0".27 ± 0".04; θ = 358° ± 5°.

A key finding, resulting from the image reconstruction, was that the new source is located north of the astrometric position for T Tauri, distinct from the southern infrared and radio source. A second set of observations from the Mount Wilson 2.5 m run in 1984 October confirmed the existence of the northern source and allowed determination of some of its physical characteristics. Table 1 summarizes the results from the different observations.

The angular resolution obtained from these data sets is better than 0".10, and the companion is unresolved at this scale. The brightness of the companion is too great relative to T Tauri to be explained either by reflection from a nearby cloud or by production from a jet; however, these possibilities cannot be completely ruled out without additional observations. We believe it more likely that the second source is a stellar companion.

The bolometric corrections for main-sequence stars are not generally applicable to pre–main-sequence stars without including, for example, the star's infrared excess. The bolometric luminosity of the northern companion may not be directly derived using only its visual magnitude difference from the primary. However, from the measured magnitude differences as a function of color, a probable spectral class for the companion was determined. Spectral classification from the data is not trivial since (1) the strong Hα emission is included in the bandpass of the filters for two of the data sets, and (2) the difference in extinction between the two components is unknown. For our calculations, the assumptions were that both stars had the same extinction, and, to first approximation, both stars could be represented as blackbodies. The color temperature of T Tauri has been estimated by Cohen and Kuhi (1979) to be 5000 K (K0–K1 spectral class). The measured magnitude differences yield a temperature for the companion of 3000 ± 200 K. The range of temperature reflects the accuracy of the magnitude difference estimates and corresponds to spectral types from M4 to M8. With this determination of spectral type, some of the physical characteristics of the companion may be derived, using the convective-radiative

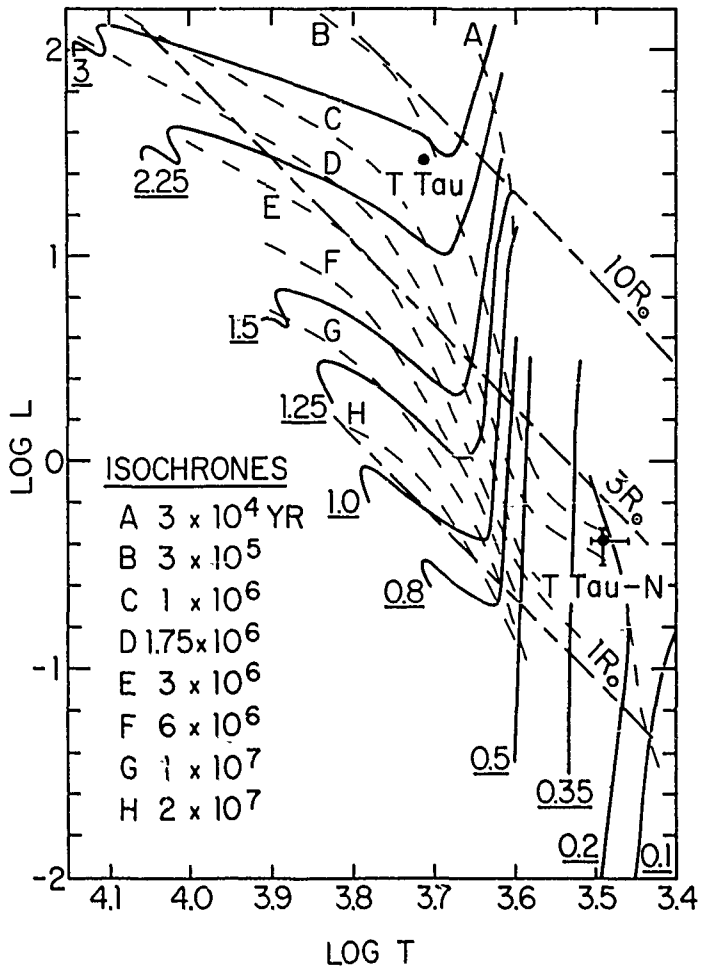

FIG. 2.—Evolutionary diagram for pre-main-sequence stars (from Cohen and Kuhi 1976) with T Tauri (north) and T Tauri (astrometric) plotted on it. Error bars introduce a possible range of temperatures and indicate the corresponding range of bolometric luminosities.

evolutionary tracks given by Cohen and Kuhi (1979) for pre-main-sequence stars.

Figure 2 is the evolutionary diagram from Cohen and Kuhi (1979) with T Tauri and its companion plotted on it, assuming coeval formation of the two sources (isochrone between 3×10^5 and 10^6 yr). The error bars show the range of temperatures and the corresponding range of bolometric luminosities. The bolometric luminosity of the companion is between 0.3 and 0.5 $L_\odot$. The mass and radius of the companion may be extrapolated as 0.2–0.35 $M_\odot$ and 2.5 $R_\odot$, respectively. If this estimate is correct, this would be one of the least massive pre-main-sequence stars yet detected.

V. DISCUSSION

The discovery of this new source in the T Tauri system raises as many questions as it answers. If both this source and the southern source are stellar companions to T Tauri, the geometry of the system is unexpected; dynamics of triple systems do not allow stable orbital spacings closer than about 5 : 1. Therefore, the near equal spacing of this system would have to be a projection effect, or the system would have to be young enough not to have reached dynamic equilibrium. The near alignment of the three sources is also surprising. Further observations of both the northern and southern sources are clearly needed. Measurement of the spatial distribution of the Hα emission is required in order to verify the estimated spectral type of the northern source and to rule out the possibility that its emission is produced by a jet, since the output of a jet in the red is almost entirely in Hα (Mundt and Fried 1983). The two observations made with filters that include the Hα line at 659 and 673 nm yield magnitude differences which are identical within the error bars, which is not consistent with the strong Hα emission from a jet. The infrared speckle observations reported to date do not have sufficient angular resolution to have detected the northern source. New high angular resolution infrared observations and high-sensitivity radio observations of both the northern and southern sources would be very useful.

We wish to thank K. Hege, C. Papaliolios, and S. Ebstein for their aid in the Steward observations. We are indebted to Jacqueline Fischer, who suggested and encouraged our T Tauri observations, and we wish to thank L. Hartmann, M. Simon, and P. Schwartz for many helpful discussions. Finally, we acknowledge the ongoing interest and support of Dr. Henry Radoski of the Air Force Office of Scientific Research. This work was funded under grant AFOSR-81-0055 from AFOSR.

REFERENCES

Cohen, M., and Kuhi, L. V. 1979, *Ap. J. Suppl.*, **41**, 743.
Dyck, H. M., Simon, T., and Zuckerman, B. M. 1982, *Ap. J. (Letters)*, **255**, L103.
Lozinskii, A. M. 1949, *Perem. Zvezdy*, **7**, 76.
Mundt, R., and Fried, J. W. 1983, *Ap. J. (Letters)*, **274**, L83.
Nisenson, P., and Papaliolios, C. 1983, *Optics Comm.*, **47**, 91.
Papaliolios, C., Nisenson, P., and Ebstein, S. 1985, *Appl. Optics.*, **24**, 287.
Rydgren, A. E., Strom, S. E., and Strom, K. M. 1976, *Ap. J. Suppl.*, **30**, 307.
Schwartz, R. D. 1975, *Ap. J.*, **195**, 631.
Schwartz, P. R., Simon, T., and Howell, R. R. 1984, *Ap. J. (Letters)*, **280**, L23.

M. KAROVSKA, P. NISENSON, R. NOYES, and R. V. STACHNIK: Harvard-Smithsonian Center for Astrophysics, 60 Garden Street, Cambridge, MA 02138

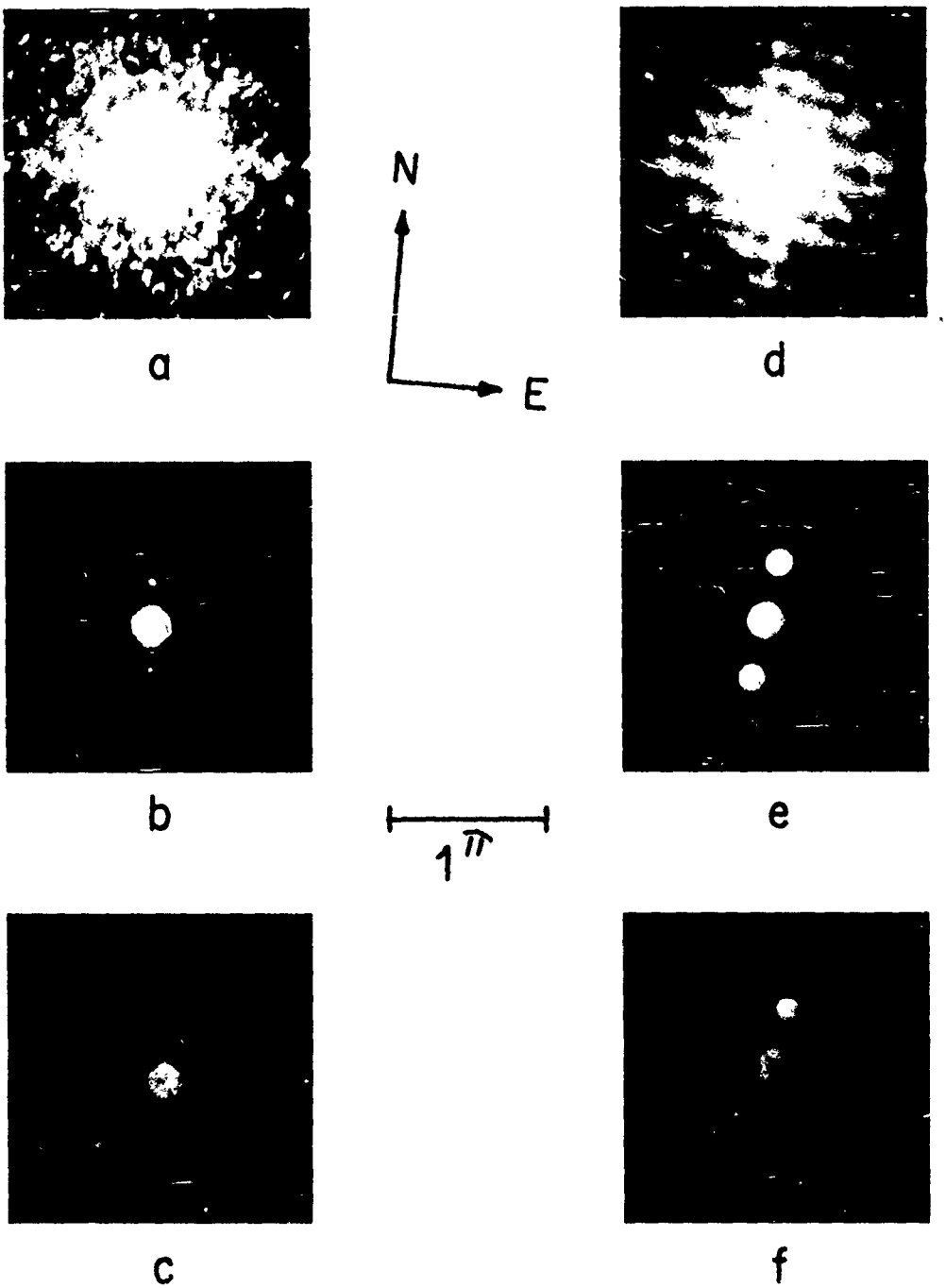

FIG. 1.—(*a*) Power spectrum, (*b*) autocorrelation, and (*c*) image reconstruction for T Tauri from data recorded on the Steward Observatory 2.25 m telescope in 1983 November. Due to the large magnitude difference between T Tauri (north) and T Tauri (astrometric), the near-horizontal fringes in the power spectrum are very low contrast, and the primary source is heavily overexposed in the image and autocorrelation. For comparison, the (*d*) power spectrum, (*e*) autocorrelation, and (*f*) image of the 8th and 9th mag binary SAO 93840 are shown (data recorded on the same observing run).

APPENDIX
F

ON THE α ORIONIS TRIPLE SYSTEM

M. Karovska, P. Nisenson, R. Noyes
Harvard-Smithsonian Center for Astrophysics
and
F. Roddier
National Optical Astronomy Observatories

ABSTRACT

Detection of two close optical companions to the red supergiant α Ori was accomplished in November, 1983, on the Steward Observatory 2.25 meter telescope. A new two-dimensional photon counting camera (the PAPA detector) was used for data recording, and speckle imaging was used for image reconstruction. The closer of the two sources is located at 0.06 ± 0.01 arcsecond from α Ori (P.A. = 273°), the more distant at 0.51 ± 0.01 arsecond, (P.A. = 278°). The magnitude differences with respect to the primary, measured at 656.3 (Hα) and 656.8 nm (red continuum) are 3.0 and 3.4 for the close, and 4.3 and 4.6 for the distant source, respectively. This observation confirms the reality of the two sources which has been reported in previous work. Our analysis favors an interpretation in which the two optical sources are stellar companions to α Ori. Strong support for the existence of the close stellar companion was found in the polarization data obtained by different observers for α Ori. A periodicity of about 2.1 years was found in the time dependent variations in the position angle of the plane of polarization, which appear to reflect the orbital motion of the close

companion. The observed polarization can be interpreted as being due to a systemic asymmetry created by the close companion orbiting α Ori inside its extended dust envelope.

I. INTRODUCTION

α Ori (Betelgeuse), a supergiant star classified as M2 Ia-Iab has been intensively analyzed by a variety of techniques. Observations accumulated for more than a century create an ensemble of data (magnitudes, colors, spectra, polarization measurements, interferometric measurements and many others) showing the extremely complex signature of this star.

Goldberg (1979) proposed an empirical model for the morphology of the atmosphere of α Ori. Following his idea, a "visible" part of the star is comprised of a photosphere and an envelope of gas and dust in expansion. An intermediate zone, identified as a stellar chromosphere, forms a bridge between the photosphere and the dust envelope.

It is a non-trivial problem to attribute an accurate spatial scale to this model using the photospheric radius as a unit. Direct angular diameter measurements of this supergiant using different techniques appear to be wavelength and time dependent (White, 1980). Tsuji (1978) interpreted these measurements as being highly affected by the presence and distribution of scattering dust in the circumstellar shell, implying that they do not always accurately estimate the photospheric diameter of the star. Tsuji's spectrophotometric estimation of the photospheric angular diameter is 41 ± 3 milli-arcseconds (mas). Similar values were proposed by White (1980),

Ricort et al (1981), and Roddier and Roddier (1983). In our calculations, we adopt a value of 40 mas for the photospheric angular diameter. In this picture, the stellar chromosphere extends to several stellar radii from the photosphere and its upper layers are in close contact with the lower part of a dust and gas envelope which extends to several hundred stellar radii.

The linear photospheric radius can be calculated using 20 mas as the angular radius combined with the distance to α Ori. The errors in trigonometric parallax measurements are comparable with the measured value of the parallax for α Ori, so instead we adopted the photometric value of 95 pc (White, 1980; Sky Catalogue, 2000) and thus estimated its linear photospheric radius to be about 400 solar radii (1.9 a.u.). For our calculations, we shall adopt the value of 20 $M_{\odot}$ for the mass of α Ori as estimated by Weymann (1962).

α Ori is characterized by pronounced variability encompassing most of its observed parameters. The star has been classified as a semi-regular variable (SRc). Its light and radial velocity curves exhibit variability on two different time scales: a long period variation of 5.78 yrs (Jones,1928) and, superposed on this "irregular fluctuations" having a time scale of several hundred days (Stebbins, 1931). The variable character of the radial velocity of α Ori was delineated by Plummer (1908). Assuming the star to be a spectroscopic double (period=6 yrs), Bottlinger (1911) calculated an orbit. The possibility of α Ori

being a double star was rejected in later works (Sanford, 1933; Spitzer, 1939; Adams, 1956), and the variations in the radial velocity curve were attributed to intrinsic variability of the star.

The renaissance of the idea that α Ori is not a single star dates from the discovery of a possible companion through observations carried out in February,1982 using pupil plane interferometry at the NSO Mcmath 1.5 meter telescope (Karovska, 1984; Roddier, Roddier and Karovska, 1984). The position angle of the companion was either 85° ± 5° or 265° ± 5° (the 180° ambiguity being inherent in interferometry) and the separation was 0.5 arcsecond. The magnitude difference between the primary and the companion was estimated to be between 3.5 and 4.0 at a wavelengtRh of 530 nm. In addition, Karovska (1984) inferred the possible existence of a second companion from an image reconstruction using the Maximum Entropy Method. The location of this second source was 0.04 arcsecond from α Ori, at a position angle of 325° ± 5°. However, this was a super-resolution result, so this evidence for a close second companion was by no means definitive.

In November, 1983, at the Steward Observatory 2.25 meter telescope, new observations were obtained that strongly indicated the existence of two companions to α Ori. One of the detected companions was located at position angle 278° ± 5° and distance 0.51 ± 0.01 arcsecond, thus providing strong confirmation of the

reality of the more distant companion. The other companion lay at position angle 273° ± 5° with a separation from the primary of 0.06 ± 0.01 arcsecond, and thus could be the same object inferred by Karovska (1984) from the earlier data only if the position angle had changed in the interim by about 308° in a counter-clockwise direction or 52° in a clockwise direction.

Recognizing that the initial inference of a possible close companion was a marginal detection, we have nevertheless explored the consequences if a single object was in fact located at the cited positions at the two observing times, and conclude that this would be consistent with a stellar body orbiting α Ori at a mean distance of 2.5 stellar radii and a period of about 2 years. We have analyzed available polarization data (Hayes, 1984) and find that these data are also consistent with the existence of a close companion. In addition, observations of asymmetries in other interferometric data and of apparent mass ejections from α Ori in previous decades lend support to the existence of a close companion, whose periodic interaction with α Ori give rise to a number of phenomena associated with the star.

This paper reports the results of the November 1983 observation as well as the analysis of polarization data which appear to be consistent with the existence of the close companion to α Ori.

II. THE OBSERVATIONS

Speckle observations of α Ori were carried out on 15 and 16 November, 1983, with the Steward Observatory 2.2 meter telescope. The observations were made using the Precision Analog Photon Address (PAPA) detector (Papaliolios et al,1985), a two-dimensional photon counting sensor which records a catalog of sequential photon positions. The PAPA camera records data at a rate of 100,000 photons/s with a field size of 256x256 pixels. The photon addresses are encoded on a video carrier and stored using a conventional VCR for later digital processing. The speckle process requires that the images be magnified so that the diffraction limit of the telescope correctly sampled by the recording sensor (a minimum of two pixels per resolution element), that the effects of atmospheric refraction be corrected, and that the bandpass of the light be restricted to meet coherence requirements. For these observations, we used an optics package developed by K. Hege and J. Beckers. A birefringent filter developed for differential speckle interferometry (Beckers, *et al.*, 1984) was used for recording the α Ori data. This filter produces two images side-by-side each having a bandpass of 0.125 nm with one image centered on Hα and the other shifted to the red by 0.5 nm. The two images are recorded simultaneously on the detector. During the numerical processing of the data, the two images may be separately analyzed or, in the

differential mode, the entire field may be processed yielding cross product terms that could yield super-resolution information. In this paper, we discuss only results from conventional processing of the two separate images.

III. DATA PROCESSING

The photon addresses are first converted to conventional digital data through a buffered interface to a Data General Nova computer. These addresses are then divided into subsets (or frames) whose length matches the characteristic correlation time of the atmosphere. The testing of different correlation times allows a maximization of the signal-to-noise in the integrated result. This is important since the correlation time may vary widely throughout the night, resulting in a substantial reduction in signal-to-noise if fixed frame times are used (which would be the case for standard framing cameras). Typical correlation times range from a few milliseconds to tens of milliseconds. Individual images are constructed from the photon list simply by incrementing the addressed array position. The Fourier transform for each image is computed and the complex correlation arrays required for speckle image reconstruction (Nisenson and Papaliolios,1983) are calculated and integrated. Correction for the atmospheric and telescope transfer functions are performed by

using data recorded for an unresolved reference star. This star should be located close in angular position and time as possible to the stellar data recording. This approach insures that, in almost all cases, the long term atmospheric statistics are similar for the two data sets. Deconvolution by the reference star results in enhancement of the high angular frequences in the reconstruction. Many of the problems that made accurate speckle image reconstruction difficult for faint sources, in particular the correction for the photon noise bias (Nisenson and Papaliolios, 1983), are completely eliminated for data recorded with the PAPA detector. The fundamental linearity and unlimited dynamic range of the photon counting camera allows a far more accurate reconstruction of binaries with large magnitude differences and low contrast stellar features than was ever possible with the conventional detectors used in speckle interferometry.

IV. RESULTS AND ANALYSES

a) Interferometric Data

The existence of two optical sources in proximity to the red supergiant α Ori was confirmed by the November 1983 observations made at Steward Observatory. The result of data

processing was the detection of two low contrast fringe patterns in the power spectrum oriented in slightly different directions. The low contrast of the fringes indicates a large difference in intrinsic brightness of the primary and secondary sources. The power spectrum, autocorrelation, recovered phase and reconstructed image (Fig. 1), demonstrate the reality of the companions and allow accurate determination of their separation from the primary, position angle, and magnitude differences.

The closer of the two sources was found to be at 0.06 ± 0.01 arcsecond from the primary and the second more distant source, at 0.51 ± 0.01 arcsecond. An essential result of speckle image reconstruction is the elimination of the 180° ambiguity normally associated with interferometry, allowing correct positions of the sources to be determined. The distant source was located at a position angle of 278° ± 5°, close to one of the two possible positions (265° ± 5°) derived from the February 1982 data. The derived position angle for the close source is 273° ± 5°, substantially different from that inferred from the observations of February 1982, (325° ± 5°).

α Ori was observed simultaneously through two close spectral windows centered at 656.3 nm (Hα) and 656.8 nm (red continuum). The bandpass was the same for both observations: 0.125 nm. The derived magnitude difference between the primary and the close source was 3.0 ± 0.1 in Hα and 3.4 ± 0.1 in the continuum. For the distant source this difference was higher:

4.3 ± 0.1 in Hα, 4.6 ± 0.1 in the continuum. The fact that for both companions the Hα magnitude difference is about 0.3 magnitudes smaller than the off-band magnitude difference suggests that the equivalent width of Hα is about the same for both companions and smaller than the equivalent width for the primary.

The high intrinsic brightness of α Ori ($M_V \approx -5$, White, 1980) and the measured magnitude differences imply a substantial intrinsic brightness for both companions. The high brightness of these sources and the fact that they are not resolved (the angular resolution obtained from our data is better than 0.1 arcsecond) suggest that they cannot be interpreted as reflections from dust clouds in the extended envelope of the supergiant. The presence of large structures (such as prominences) extending above the surface has been also considered as a possible explanation. Since the distant source would be located at a distance of about 25 stellar radii, any explanation other than it being a stellar companion is unlikely. This argument is not valid in the case of the close optical companion. We can not rule out the cause of the change in position angle of the close source from 325° in 1982.1 to 273° in 1983.9 as being either due to the rotation of a feature extending above the surface of α Ori, or the appearence of a new feature at a different position angle. However, the high brightness of the sources relative to α Ori (in the continuum, as well as in Hα) and the fact that they are not angularly resolved with the 2.25 meter telescope suggest

that a prominence-like structure is unlikely. On the other hand, the high brightness of these unresolved sources could be due to their stellar nature.

If the companion is a stellar object, then the inferred change in position angle of the close source from 325° in 1982.1 to 273° in 1983.9 is due to its orbital motion. A preliminary estimate of the orbital period can be obtained from the detected change in position angle between the two epochs of observation assuming that the orbit is circular and situated in the plane of the sky. Since the sense of the orbital motion is not known a priori, possible changes in the position angle could be: $\Delta\theta_1$ = 52° or $\Delta\theta_2$ = 412° (clockwise motion) or $\Delta\theta_3$ = -308° (counter-clockwise motion). Calculated periods are respectively: P_1 = 12.5, P_2 = 1.6 and P_3 = 2.1 years. From Kepler's third law, the sum of the masses of α Ori and the close companion can be calculated for each of these periods and a value for the linear radius of the orbit. Using the adopted value of 95 pc for the distance to α Ori and a mean value of the two interferometric measured distances (0.05 arcsecond), we estimate a linear radius of the orbit of about 4.75 a.u. This leads to sums of the masses of 0.7, 41.9 and 24.3 $M_\odot$, respectively for P_1 ,P_2 and P_3. The first value, 0.7 $M_\odot$, can be eliminated immediately since it is much too low. The large magnitude difference between the close companion and α Ori implies that its mass is substantially smaller than that of the primary. However, the value of 41.9 $M_\odot$

together with the adopted mass of about 20 $M_\odot$ for α Ori, would imply that the mass of the companion is comparable to that of α Ori, so the period of 1.6 years can also be dismissed. Therefore, we consider counter-clockwise orbital motion with a period of 2.1 years and a sum of masses of about 24 $M_\odot$ as a more likely solution.

Independent supporting evidence for the existence of the close stellar companion was also found in the polarization data. Analysis of the polarization data strongly suggests that the orbit is elliptical, not circular. This analysis, plus the calculated orbit will be discussed in section IVb.

Some other interferometric observations appear to be consistent with the existence of the close companion. Goldberg at al. (1981) observed α Ori using speckle interferometry and reconstructed its image in 650 nm continuum radiation. They detected an "unresolved bright feature" near the SW limb of the star at position angle 208° ± 5°. Roddier and Roddier (1983) observed α Ori 2.5 months before Goldberg *et al.* in the 534.8 nm continuum using pupil plane interferometry. They detected a high frequency excess in the two dimensional map of the fringe visibility and interpreted this excess as due to a bright feature on the stellar limb (photospheric radius of 0.02 arcsecond) at position angle 202°. The resolution limit for this observation is close to 0.03 arcsecond which shows that the observed structure could be located anywhere between 0.02 and 0.05

arcsecond. It seems plausible that Goldberg *et al.* and Roddier and Roddier actually observed the close companion or the consequence of its interaction with the stellar surface. Later (section Vc.) it will be shown that the position angles of these bright features match well the predicted position on the calculated orbit for the close companion.

The detected change in position angle of the distant companion is a counter-clockwise displacement of $\Delta\theta \approx 13°$. It is difficult to conclude from these data whether this change corresponds to the companion's orbital motion, since the position angles are not significantly different, given the observational errors. The angular separation did not change within the error bars for the two observations. An orbital period of order 65 years (leading to $\Delta\theta \approx 10°$) would be expected for a companion of a moderate mass having a circular orbit with radius of about 48 a.u. (angular radius 0.5 arcsecond and distance 95 pc). This would be consistent with our data if the orbit is counter-clockwise - that is, in the same sense of rotation as the inner companion.

b) Polarization Data

A number of measurements of the polarization of α Ori were

carried out from 1968 through 1981 by Dyck and Jennings (1971), Serkowski (1971) and Tinbergen (1981). α Ori, like most late-type luminous stars, has substantial (up to 1%) intrinsic polarization. Since 1979 the polarization has been monitored regularly, except during the spring and summer interregnums (Hayes, 1984). A particularly interesting aspect of these data is that the degree of polarization as well as the position angle exhibit a wide range of variations with time. Hayes (1984) pointed out that the variation of linear polarization observed in the optical continuum (B band) is characterized by "ordered (as opposed to stochastic) structures". The time-scale of these structures reported by Hayes is of the order of several hundred days and is similar to the time-scale of the photometric changes. Figure 2 shows the B-magnitude measurements from 1979.7 to 1980.3 (Krisciunas, 1982; Guinan, 1984) and the degree of polarization data for the same period (Hayes, 1984).

Several plausible interpretations of the origin of large changes in the polarization of α Ori have been proposed (Hayes, 1984; Schwartz and Clarke, 1984): changes in the circumstellar envelope due to mass loss, Rayleigh scattering in the photosphere of α Ori, presence of few large-scale photospheric convective cells,etc. Attempts were made to find the mechanism(s) which could account for the wide range over which the α Ori polarization position angle changes. One of the proposed mechanisms was scattering of light on matter co-rotating with α Ori as a consequence of binary motion (Hayes, 1984). Several

reasons led Hayes to dismiss this mechanism as an explanation of the behavior of the position angle: (1) The lack of convincing evidence for short-term periodicity in the photometric or radial velocity data; (2) The polarization does not show periodicity when plotted in th Q-U Stokes parameter frame; (3) The characteristic time-scale of variations in the position angle (several hundred days), if interpreted as a period of a stellar companion orbiting α Ori, implies a semi-major axis which is smaller than the radius assumed by Hayes of 633 solar radii (Weymann, 1977).

Observations of the two optical sources close to α Ori and their interpretation as stellar objects suggested that they may also give clues to the interpretation of polarization data. The results of the wide-band (B filter) linear polarimetry carried out during four consecutive observing seasons, from 1979 to 1983 by Hayes provide the longest continuous data set available for analysis. Measured values for the degree and position angle of polarization are given by Hayes (1984).

The time-dependent polarization data were examined for periodic behavior related to the orbital motion of the close companion. The first step in our analysis was to display the polarization angle (thirty day mean) as a function of time, taking into account the 180° ambiguity characteristic of these measurements. The result is presented in Fig. 3. The straight line is a linear least-square fit to these data, plus additional

unpublished data for the period August, 1983 to April, 1984, kindly supplied by Dr. D. Hayes (Hayes, 1985). The individual data points used in the fit were weighted inversely with their estimated error. The slope of the straight line corresponds to a period of 25 months (2.08 years). A least-square fit to the data (straight line on Fig. 3) shows a periodicity of 25 months (2.08 yrs.). The fitted line was subtracted from the data and the resulting curve revealed the same periodicity. Deviations of the data points from the linear least-square fit are statisticaly significant and can not be interpreted as observational errors.

The degree of polarization appears to manifest periodicity as well (Fig. 2*b*). The period is approximately half of that which has been detected for the position angle. The same periodicity (1.05 ± 0.02 yrs.) was detected in the light curve of α Ori as a result of Fourier analysis of 60 years of data accumulated by the American Association of Variable Star Observers (A.A.V.S.O.), and presented by Goldberg (1984), (Karovska, 1984).

The presence of two periodicities in the polarization data (the period of variation of the polarization angle being twice the period of variation of the degree of polarization) is not an unusual phenomenon for close binary systems (Daniel, 1981; Rudy and Kemp, 1978; McLean, 1980). Daniel suggested that tidal distortion of the primary could account for the periodic behavior of the light and the degree of polarization variations. The

observed behavior of the α Ori polarization strongly suggests that it may be interpreted as being a consequence of the binary nature of α Ori. If this is the case, the orbital period of the companion will be equal to the period of the polarization angle variations (2.1 years). The half- orbital period in the variation of the degree of polarization and photometric brightness may be explained by the relative position of the tidal distortion of the primary and the observer (if the orbit is not in the plane of the sky). This period is in perfect agreement with the period we estimated for the close companion from interferometric data. Furthermore, the polarization position angle turns in the counter-clockwise sense, which coincides with the sense inferred for the orbital motion of the close companion.

The short periodicity in the variations of the polarization angle with time makes it unlikely that these variations could be due to the rotation of the large-scale surface features. From the adopted value of 400 solar radii for the radius of α Ori, a rotation period of 2.1 years would imply an equatorial velocity of about 27 km/s which appears to be very high for a single late-type supergiant.

Another point to be considered is the possible mechanism for producing polarized radiation in the α Ori system. Rayleigh scattering (which varies as λ^{-4}) was suggested as a predominant mechanism for the polarized radiation in the atmosphere of α Ori (Tinbergen et al, 1981). Our study of the wavelength dependence

of the degree of polarization (polarization data from Dyck and Jennings, 1971; Serkowski, 1971; Tinbergen et al, 1981) shows that the predominant mechanism is Mie scattering by dust grains, which can only occur in the extended envelope of the supergiant. Least squares fit to three of the data sets by a linear function of $1/\lambda$ (Mie scattering) are shown in Fig. 4. Thus, we are led to consider an interpetation of the changing polarization angle and degree that involves temporal variations in the interaction of radiation with dust in the extended envelope.

V. DISCUSSION

a) Interpretation of Polarization

There is no question that dust grains are present in the circumstellar environment of α Ori. The excess radiation at 11 μm in the spectrum of this star is indicative of the presence of silicate particles. Dust has also been detected at several tens of stellar radii by interferometric measurements in the infrared (McCarthy *et al.*, 1977; Sutton *et al.*, 1977) and by direct infrared imaging (Bloemhof *et al.*, 1984; 1985). Observations in the visible (speckle interferometry: Ricort *et al.* 1981; and pupil plane interferometry: Rodder and Roddier, 1983,1985; Karovska, 1984) showed the presence of dust within a few stellar radii from the surface of the star. These observations are in

agreement with the results of Draine's (1981) study of dust formation. Draine has shown that clean silicate grains can survive close to the stellar surface and he predicted a minimum condensation radius of 1.8 stellar radii for α Ori. Such clean silicate grains close to the stellar surface would enhance the amount of scattered radiation in the visible (Tsuji, 1978) and consequently, the degree of polarized light. The fact that the degree of polarization is coupled to the light variations of α Ori (see Fig. 2) also indicates the presence of polarizing particles close to the star.

We are led to a picture in which the close companion orbits α Ori within its extended chromosphere and inside its extended dust and gas envelope, thereby creating a systemic asymmetry responsible for the observed behavior of the polarization, presented in schematic form in Fig. 5. The polarization may be interpreted as being caused by Mie scattering of the light from the companion itself or from the primary which has been rendered asymmetric by tidal distortion due to the proximity of the companion. If this interpretation is correct, the shape of the curve giving the time dependence of the angle of polarization should reflect the geometry of the orbit and the geometry of the scattering medium.

We may draw some conclusions about the source of the polarization variations from the detailed shape of the polarization curve shown in Fig. 3. First, let us assume that

the scattering medium is spherically symmetric. In that case, it is easy to rule out an orbit for the companion that is circular and lies in the plane of the sky, for the resulting time variation of polarization angle would then be linear, rather than exhibiting the nearly periodic departures from linearity seen in Fig. 3. It is possible that these departures could result from a large eccentricity e or a large inclination i of the orbit, or some combination of the two. We have tried to match the polarization curve with such orbits, and found that, under the assumption of a spherically symmetric scattering medium, there is no combination of e or i which matches the polarization curve without entailing one of the two following unacceptable conditions:

(a) the eccentricity is so high that the orbit would pass inside the photosphere of α Ori, or

(b) the inclination is so large that Doppler shifts of the primary star would be detectable in the spectrum even for mass ratios for the primary to secondary as large as ten.

It is also the case that for high values of eccentricity or of inclination, the two interferometric positions for the inner companion discussed above cannot be reproduced with a 2.1 year orbital period.

Therefore, we are led to the interpretation that the

amplitude of the polarization curve is due at least in part to an asymmetry of the scattering medium; such an asymmetry, when combined with an elliptic orbit characterized by only moderate eccentricity and inclination, can lead to a predicted polarization curve which matches the observations without violating either of the above constraints.

Given the possibility of an non-spherically symmetric scattering medium, there are then many hypothetical orbits which can fit the two positions of the companion within the error bars. The number of plausible orbits can be reduced by adopting the parameters which have been determined from the polarization angle data: a period of 2.08 ± 0.08 yrs., epoch = 1980.4 ± 0.1, position angle of the periastron, with respect to North, 60° ± 10°. For the semi-major axis we adopted 0.05 arcsecond, the mean value of the interferometrically measured distances of the companion; at the adopted 95 pc for the distance to α Ori, the length of the semi-major axis is then approximately 4.7 a.u. Combined with the period of 2.08 yrs., these values imply that the sum of the masses of α Ori and its close companion is about 24 $M_\odot$. Using the adopted value of 20 $M_\odot$ for α Ori, the mass of the binary companion would be approximately 4 $M_\odot$. At this point, the only free parameters left are the eccentricity and the inclination of the orbit. A very good fit to the measured positions of the companion has been obtained by an orbit characterized by these parameters: P=2.08 yrs., T=1980.4, a=4.7 a.u., Ω=60°, ω=0°, e=0.35, i=30°. There is a 180° ambiguity in

the position angle of the ascending node and, consequently in the longitude of the periastron. However, this orbit has to be considered with caution, since its determination is based mostly on parameters originating from the interpretation of the polarization data. New high resolution observations of the α Ori system are necessary for a more accurate determination of the orbit.

b) The Dust Envelope

When the exact form of the orbit of the companion is accurately determined, interpretion of the shape of the time dependence of the polarization angle should allow a determination of the geometry of the scattering medium. The observations of α Ori based on interferometric techniques as well as direct IR imaging indicate the presence of strong asymmetry in the dust envelope surrounding this star. Dust grains which form the inner boundary of the extended shell appear to be the most efficient scattering medium in the star envelope (Lefevre *et al.*, 1982, 1983). Thus, the shape of the polarization angle curve will be strongly influenced by the geometry of the inner part of α Ori's envelope.

An interferometric image reconstruction of α Ori in the visible performed by Roddier and Roddier (1985) shows that in November, 1980 there existed an asymmetric circumstellar

structure at 1 to 1.5 stellar radii from the surface of the star. Karovska (1984) inferred from the February 1982 McMath data that at that time there existed a much fainter feature at 2-2.5 stellar radii, which she interpreted as an outward-expanding residue of the structure observed by Roddier and Roddier 15 months earlier. The apparent fading of this dust "envelope" may explain why it was not detected in our more recently recorded interferometric data.

Goldberg (1984) pointed out that during the last 60 years an unusually large, rapid decrease in the radial velocity of α Ori followed by short-lived drop in brightness occured several times. He suggested that these events may be connected with the star's pulsation: the instabilities in the atmosphere would "trigger mass ejection and the formation of dust grains". In order to examine a possible connection of these instabilities with the orbital motion of the close companion, the epochs of the unusually large decreases in radial velocity were compared with the corresponding epochs of the close companion's periastron passage. The epochs we determined from the data presented by Goldberg (1984) are: 1926.6, 1938.8, 1944.9, 1961.5, 1978.3 (± 0.2 yrs.). Using the epoch (1980.4 ± 0.1) and the period (2.08 yrs) determined from polarization data, the times of the periastron passage nearest the times when the five events took place were calculated: 1926.3, 1938.8, 1945.0, 1961.7 and 1978.3 (± 0.1 yr.). The extremely close agreement between measured and predicted epochs seems to eliminate any possibility of

coincidence.

The dust shell observed at 1 to 1.5 stellar radii in 1980.9 and 15 months later at 2 to 2.5 stellar radii may have been the result of an outburst from the primary during the companion's periastron passage in 1978.3. The mean velocity of expansion of the ejected matter would then have been about 4 km/s for the first observation and about 5 km/s for the latter. If the mass loss of the star is known, the flow velocity, v at the condensation point is given by Draine (1981):

$$v \lesssim 7 \left[\dot{M}_{-6} L_4^{-1/2} (T/3000K)^2 (R/r)\right]^{1/2} km\,s^{-1}$$

where $\dot{M}_{-6} \equiv (\dot{M}/10^{-6} M_\odot\ yr^{-1})$, $L_4 \equiv (L/10^4 L_\odot)$, R≡stellar radius, r≡minimum condensation radius, T≡stellar effective temperature.

We adopt a mass loss rate for α Ori of $10^{-6} M_\odot\ yr^{-1}$ (Reimers, 1975) and its luminosity as $4.5\ 10^{-4} L_\odot$ (assuming M_b=-6.9, White 1985, private communication). The adopted effective temperature is 3600 K (Scargle and Strecker, 1979). With 1.8 stellar radii for the minimum condensation radius (Draine, 1981), the upper limit of the flow velocity during grain nucleation is about 4 km/s. This value is consistent with the previously calculated expansion velocities. Once the dust grains are formed, they may well have been accelerated by radiation pressure to a terminal velocity of about 10 Km/s (Goldberg, 1979). The drop in brightness which follows the minimum in radial velocity

may correspond to the time when the ejected gaseous matter condenses into grains and the grains become optically thick in the visible (Goldberg, 1984).

Mass ejection from the primary during the companion's periastron passage can account for the origin of dust and gas shells observed in the circumstellar environment of α Ori (Honeycutt *et al.*, 1980; Bloemhof *et al.*, 1984). The fact that outbursts do not occur during each periastron passage suggests that a substantial ejection of mass may occur only when the periastron epoch is close in time to the epoch of the maximum expansion velocity of α Ori, i.e. the minimum of its radial velocity relative to the earth. The spectacular decreases in radial velocity occur just after the time of the minimum in the pulsational radial velocity curve (period = 5.8 years, Goldberg,1984). When periastron passage and maximum pulsational expansion do not occur close together, one might expect to observe alternative outfall and infall of matter from the primary due to the tidal effect caused by the companion each time it passes periastron. Some observations (Boesgaard, 1979; Van der Hucht *et al.* 1979; Quercy and Quercy, 1985) seem to indicate such behavior of the material located between the surface of α Ori and 1-2 stellar radii distance.

The previous discussion leads to the conclusion that the structure which has been observed close to the stellar surface (Roddier and Roddier, 1985, Karovska, 1984) can be interpreted as

a temporarily enhanced concentration of dust grains, a consequence of an outburst of matter from the primary at the epoch when the companion was in periastron. This outburst could create a supplementary asymmetry and anisotropy in the scattering medium which would be responsible for temporary fluctuations in the observed time variation of the angle and the degree of polarization. (See for example the variations in the data in Fig. 3 corresponding to epochs at the end of 1979 and the end of 1981). Such events coupled with the intrinsic long-term variability of α Ori, can explain why the polarization does not exhibit consistent periodic repetability when directly plotted in the Q-U Stokes parameter frame.

c) Other Possible Detections and the Orbit

The interferometric detections of the two bright sources close to α Ori and our study of the polarization data strongly suggest that α Ori is not a single star but a triple stellar system. It is interesting that there are no other claims of detection of the companions in past high resolution observations. However, it should be noted that the small angular distances of the companions from α Ori and the large magnitude differences between the companion stars and the primary make the detection extremely difficult. The new two dimensional photon camera we used for data recording and the techniques of speckle imaging developed for data processing appear to be a powerful tool for this kind of observation. However, as was mentioned earlier, the

bright features observed by Goldberg et al (1981), and Roddier and Roddier (1983) may be identified as the companion itself, or as a manifestation of the interaction between the close companion and the primary's photosphere.

We made an attempt to predict the position of the companion for the epochs of these observations using the orbit which has been determined in this work. The predicted position angle and distance from the primary for the epoch when Goldberg *et al.* observed α Ori are 214° and 0.059 arcsecond, respectively. For the epoch of the Roddier and Roddier observation, the predicted position angle is 196° and the distance 0.051 arcsecond (Fig. 6). The agreement of the predicted position angles and distances with the observations of the bright structures is striking.

d) Spectral Classification

The absolute magnitude of the companions at 656.8 nm may be inferred from their intensity ratio to the primary . Using the adopted absolute visual magnitude for α Ori of $M_V \approx -5$ and scaling to 656.8 nm using V - R = 1.64 (Johnson, et al, 1966), we find $M_{656.8} \approx -6.6$ for α Ori. Then, for the inner and outer companions we determine $M_{656.8} \approx -3$ and -2, respectively. Given the limited information on color dependence from the data, it is very difficult to determine the spectral class of the two companions. We assume that the companions are coeval with the

primary (age of about 10^7 years). Then, either hot early type main sequence stars or, alternatively, massive cool stars would be in agreement with the evolutionary tracks in the H-R diagram (Novotny, 1973).

However, since no indication of the presence of the companions in the spectra of α Ori has been reported, this sets some limits on the spectral class and mass of these objects. The far UV spectrum of α Ori (I.U.E. data from 120 to 300 nm) shows no indication of a continuum due to the presence of a hot companion. The two companions could be luminous, late-type giants (later than G5). This would also be consistent with their high brightness. In spite of their intrinsic brightness, their large magnitude differences from the primary would explain why their spectrum has not be seen in the visible.

The orbit suggested for the close companion ($e \approx 0.35$ and $i \approx 30°$), and its inferred mass (4 $M_\odot$), allow calculation of the amplitude of the velocity curve of the primary (≈5 km/s). Detection of a periodic (2.1 yrs) variation of the spectrum of α Ori has not been reported to date. This may be due to the fact that the radial velocity of α Ori has only been monitored irregularly (Goldberg, 1984). Also, the variation in the spectrum due to the presence of the companion may well be masked by the variations of the photospheric radial velocity of α Ori (period of 5.8 years and mean amplitude of about 6 Km/s, Goldberg, 1979). However, if α Ori is less massive than 20 $M_\odot$,

the estimated mass of the companion will increase and Doppler shifts of the spectrum of the primary will be detected unless its orbit is characterized by low eccentricity and inclination.

Another possibility for detecting companions from the spectrum is to search for energy emitted by accreting material (Kenyon and Webbink, 1984). The energy emitted by a steady state, time-independent accretion disk around a star of mass M and radius R, and for accretion rate $\dot{m}$, is given by $GM\dot{m}/2R$ (Shakura and Sunyaev, 1973), where G is the gravitational constant. We assume that, at most, 10% of the mass lost by α Ori during one year is accreted by the companion. We shall adopt the value 10^{-6} $M_\odot$/yr for the mass loss for α Ori (Reimers, 1975) which gives, for the accretion rate, $\dot{m}=10^{-7}$ $M_\odot$/yr. If the close companion is a late type giant of mass about 5 $M_\odot$ and radius of the order of ten solar radii, then the energy radiated by the accretion disk would be about 1 $L_\odot$. The emitted energy is far below the luminosity of the companion and α Ori itself, so it would not be detected in the spectrum. We note that all the assumptions made for the calculation of the accretion energy are very liberal upper limits. However, at the periastron passage of the close companion, the mass loss from the primary may significantly increase and the accretion energy may become detectable.

An intriguing question is how a few solar mass object could be coeval with α Ori. The evolutionary time for a single star

with a mass comparable to that of the close companion would be substantially longer than that for α Ori (as estimated from evolutionary tracks, Novotny, 1973). On the other hand, the proximity of the companion to the primary suggests that the evolution of each of the components can not be considered separately, and that we are actually dealing with objects which are products of the evolution of a close binary system with mass exchange.

There are many unanswered questions associated with this system. For example, why has the orbit of the close companion not been circularized during the evolutionary time of the system? Since the current orbit of the close companion appears to be totally inside the primary's chromosphere, why hasn't it decayed, causing the companion to spiral into the primary? Since α Ori is a massive star, its evolution is very rapid, so it probably has not been in its supergiant stage for very long. If this is the case, until only recently the orbit of the close companion would have been outside the primary's atmosphere where atmospheric drag would not have affected the orbit.

7. SUMMARY AND CONCLUSION

Two optical sources in the vicinity of the red supergiant

α Ori have been detected with the Steward Observatory 2.25 meter telescope using PAPA camera and the techniques of speckle imaging. The sources were identified with those suggested in 1982 and interpreted as stellar companions to α Ori. In 1983, the companions were located at 0.06 ± 0.01 and 0.51 ± 0.01 arcsecond from the primary at position angle 273° ± 5° and 278° ± 5° respectively.

Analysis of the available polarization data resulted in a discovery of periodicity in the time dependent variation of the position angle of the plane of polarization (2.08 yrs.) and of the degree of polarization (≈1 yr). The behavior of α Ori polarization is very similar to that of some close binaries, suggesting that it may be caused by the systemic asymmetry created by the orbital motion of a close companion. A period of 2.08 yrs. will then correspond to the orbital period of the companion.

Modeling of the polarization data and interferometric positions of the close companion allowed determination of a plausible orbit. This orbit was used to predict the position of the companion for the epochs when Goldberg *et al.* (1981) and Roddier and Roddier (1983) observed a bright feature on the stellar limb and interpreted this structure as a photospheric large-scale convective cell. The predicted and measured angles coincide within error bars which suggest that they actually may have observed the close companion or its effect on the stellar

surface.

Our orbit predicts that at periastron the companion passes only about half a stellar radius above the surface of α Ori, or even closer when the star is near its maximum pulsational expansion. One can expect to see many interesting phenomena when the companion is close to the photosphere of the supergiant: formation of large convective structures on the surface of the supergiant, tidal distortion of the primary, mass ejection from the primary, and possibly, the formation of an accretion disc or envelope around the companion. There is strong evidence that, when the epoch of periastron coincides with the epoch of maximum expansion velocity of α Ori, instabilities induced in the photosphere trigger mass ejection.

Further high resolution observations are very desirable in order to provide an unambiguous confirmation of the existence of these stellar objects. Future important observational goals would include:

-improved accuracy in measurement of the angular diameter of α Ori as well as the distance to this star
-determination of the spectral type of the two companions by multicolor observations
-determination of the orbits and consequently masses of α Ori and its companions
-study of possible interactions between the close

companion and the primary, particularly at the epoch of periastron

-search for indications of mass ejection and possible formation of an accretion disc or envelope around the close companion at periastron

-search for tidal distortion of the primary due to the proximity of the companion at periastron

-more accurate measurement of the angular diameter of α Ori in different colors in order to determine its wavelength and time dependencies

-search for large convective cells on the surface as predicted by Schwarzschild (1975)

-high resolution mapping of the inner boundary of the α Ori dust envelope, providing indispensible information on parameters needed for an accurate modeling of the observed polarization of the system.

In this paper, we believe we have contributed some important new information and insights into the complex nature of the α Ori system. However, there is still an enormous amount to be learned and a wide variety of observations are required, particularly when the close companion is at periastron (next occurence should be in the fall of 1986). Even more exciting will be observations at the time when the periastron epoch is close to the epoch of the pulsational radial velocity minimum.

ACKNOWLEDGEMENTS

We wish to thank S. Ebstein, K. Hege, and C. Papaliolios for their help in the Steward Observations. We are indebted to S. Baliunas, A. Dupree, L. Goldberg, E. Guinan, L. Hartmann, D. Hayes, C. Roddier and N. White for many useful discussions. Special thanks to S. Kenyon and J. Lefèvre for many important suggestions and to B. Langer for her artistic figure preparation. We also wish to acknowledge the on-going support of H. Radoski of the Office of the Air Force Office of Scientific Research under contract # AFOSR-81-0055.

References

Adams, W.S. 1956, *Ap.J.*, 123, 189.

Beckers, J.M., Hege, E.K. and Murphy, H.P. 1983, Proc. Soc. Photo-Opt. Instrum. Eng., 445, 462.

Bloemhof, E.E., Townes, C.H., and Vanderwyck, A.H.B. 1984, *Ap.J. (Letters)*, 276, L21.

Boesgaard, A. 1979, *Ap.J.*, 232, 485.

Bottlinger, C.F. 1911,*A.N.*, 88, 160.

Daniel, J.Y. 1981, *Astr. Ap.*, 94, 121.

Draine, B.T. 1981, in *Physical Processes in Red Giants*, ed. I. Iben and A. Renzini (Dordrecht: Reidel), p. 317.

Dyck, H.M., and Jennings, M. 1971, *Ap.J.*, 76, 431.

Goldberg, L. 1979, *Q.J.R.A.S.*, 20, 361.

Goldberg, L. 1984, *P.A.S.P.*, 96, 366.

Goldberg, L., Hege, E.K., Hubbard, E.N., Strittmatter, P.A., and Cocke, W.J. 1981, *SAO Special Report 392*, p.131.

Guinan, E.F. 1984, in *Cool Stars, Stellar Systems, and the Sun*, ed. S.L. Baliunas and L. Hartmann, *Lecture Notes in Physics*, 193, 336.

Hayes, D.P. 1984, *Ap.J. Suppl.*, 55, 179.

Hayes, D.P. 1985, (Private Communication).

Hirshfeld, A., and Sinnott, R.W. 1982, *Sky Catalogue 2000.0*, 1, (Sky Publishing Corporation & Cambridge University Press), p.131.

Honeycutt, R.K., Bernat, A.P., Kephart, J.E., Gow, C.E., Sandford, M.T., and Lambert, D.L. 1980, *Ap.J.*, 239, 565.

Johnson, H.L., Mitchell, R.I., Iriarte, B., and Wisniewski, W.Z. 1966, *Comm. Lunar and Planetary Obs.*, 4, 99.

Jones, H.S. 1928, *M.N.R.A.S.*, 88, 660.

Karovska, M. 1984, Thesis, *Les Observations a Haute Resolution de la Supergeante Betelgeuse, Universite de Nice.*

Kenyon, S.J., and Webbink, R.F. 1984, *Ap.J.*, 279, 252.

Krisciunas, K. 1982, *I.A.U., I.B.V.S. No. 2104.*

Lefevre, J., Bergeat, J., and Daniel, J.Y. 1982, *Astr. Ap.*, 114, 341.

Lefevre, J., Daniel, J.Y., and Bergeat, J. 1983, *Astr. Ap.*, 121, 51.

McCarthy, D.W., Low, F.J., and Howell, R. 1977, *Ap.J. (Letters)*, 214, L85.

McLean, I.S. 1980, *Ap.J. (Letters)*, 236, L149.

Nisenson, P., and Papaliolios, C. 1983, *Optics Comm.*, 47, 91.

Novotny, E. 1973, *Introduction to Stellar Atmospheres and Interiors*, (Oxford University Press), p. 319.

Papaliolios, C., Nisenson, P., and Ebstein, S. 1985, *Appl. Opt.*, 24, 287.

Plummer, H.C. 1908, *P.A.S.P.*, 20, 277.

Quercy, M., and Quercy, F. 1985, in *Fourth Cool Stars, Stellar Systems, and The Sun*, ed. M. Zeilik and D. Gibson, (New York: Springer), in press.

Reimers, D. 1975, *Mem. Soc. R. Soc. Liege*, 6e Ser. 8, 369.

Ricort, G., Aime, C., Vernin, J., and Kadiri, S. 1981, *Astr. Ap.*, 99, 232.

Roddier, C., and Roddier, F. 1983, *Ap.J. (Letters)*, 270, L23.

Roddier, F., and Roddier, C. 1985, *Ap.J. (Letters)*, 295, L21.

Roddier, F., Roddier, C., and Karovska, M. 1984, *UCLA Workshop on Mass Loss from Red Supergiants*, ed. M. Morris and B. Zuckerman (Dordrecht: Reidel), in press.

Rudy, R.J., and Kemp, J.C. 1976, *Ap.J. (Letters)*, 207, L125.

Sanford, R.F. 1933, *Ap.J.*, 77, 110.

Scargle, J.D., and Strecker, D.W. 1979, *Ap.J.*, 228, 838.

Schwartzschild, M. 1975, *Ap.J.*, 195, 137.

Serkowski, K. 1971, *Kitt Peak Obs. Cont. 544*, 107.

Schwartz, H.E., and Clarke, D. 1984, *Astr. Ap.*, 132, 370.

Shakura, N.I., and Sunyaev, R.A. 1973, *Astr. Ap.*, 24, 337.

Spitzer, L. Jr. 1939, *Ap.J.*, 90, 494.

Stebbins, J. 1931, *Pub. Washburn Observatory*, University of Wisconsin, *15*, 177.

Sutton, E.C., Storey, J.W.V., Betz, A.L., and Townes, C. H. 1977, *Ap.J. (Letters)*, 217, L97.

Tinbergen, J., Greenberg, J.M., and de Jager, C. 1981, *Astr. Ap.*, 95, *215*.

Tsuji, T. 1978, *Pub. Astr. Soc. Japan*, 30, 435.

Van der Hucht, K.A., Stencel, R.E., Haisch, B.M., and Kondo, Y. 1979, *Astr. Ap. Suppl. Ser.*, 36, 377.

Weymann, R. J. 1962, *Ap.J.*, 136, 844. Weymann, R. J. 1977, in *I.A.U. Colloquium 42, The Interaction of Variable Stars with their Environment*, ed. R. Kippenhahn, J. Rahe, and W. Strohmeier (Bamberg: Remeis-Sternwarte), p. 577.

White, N. 1980, *Ap.J.*, 242, 646.

Figure Captions

Fig. 1.- Speckle observation (Steward Observatory 2.25 m telescope, November 1983): *a* and *b* show the recovered power spectrum and phase; *c* and *d* show the autocorrelation and the reconstructed image for the distant companion; *e* and *f* show the autocorrelation and image for the close companion.

Fig. 2.- Measurements of α Ori B-magnitudes (*a*) and degree of polarization in the B-bandpass (*b*), for the period 1979.7 - 1983.3. The dashed curve represents Stebbins' (1931) photophotoelectric ephemeris with a period of 5.781 years.

Fig. 3.- Polarization P.A. as a function of time. Dashed line is the linear least-square fit to the data (dots). P and A indicate the epochs of periastron and apoastron, respectivily.

Fig. 4.- Least-square fit to the polarization degree data (dots) by a linear function of $1/\lambda$ showing that Mie scattering from dust grains is the predominant mechanism for producing polarized radiation in the α Ori system.

Fig. 5.- Schematic geometry for α Ori and its close companion. The close companion (α Ori B) orbits the primary (α Ori A) within its extended chromosphere and dust envelope. Stars indicate the positions of α Ori B observed in February 1982 and November 1983.

Fig. 6.- Possible orbit for α Ori B.

(●) - Measured positions of the companion in 1982.15 (Karovska, 1984) and 1983.88 (this work), and P.A. of the bright features observed in 1980.91 (Roddier and Roddier, 1983) and 1981.09 (Goldberg et al., 1981). The hashed area corresponds to the error bars in the measurements.

(x) - Predicted companion's positions on the orbit for the same epochs.

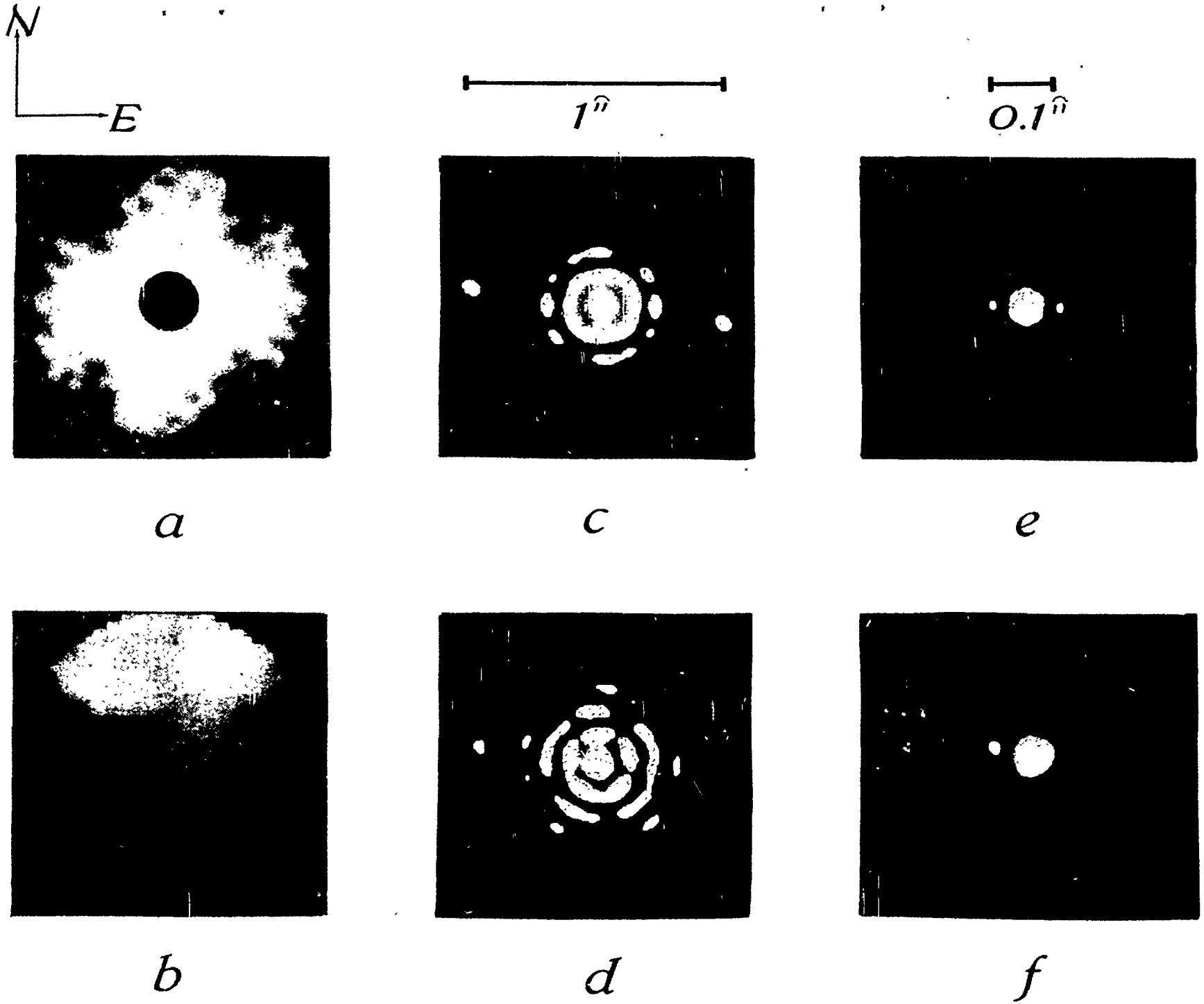

Fig. 1

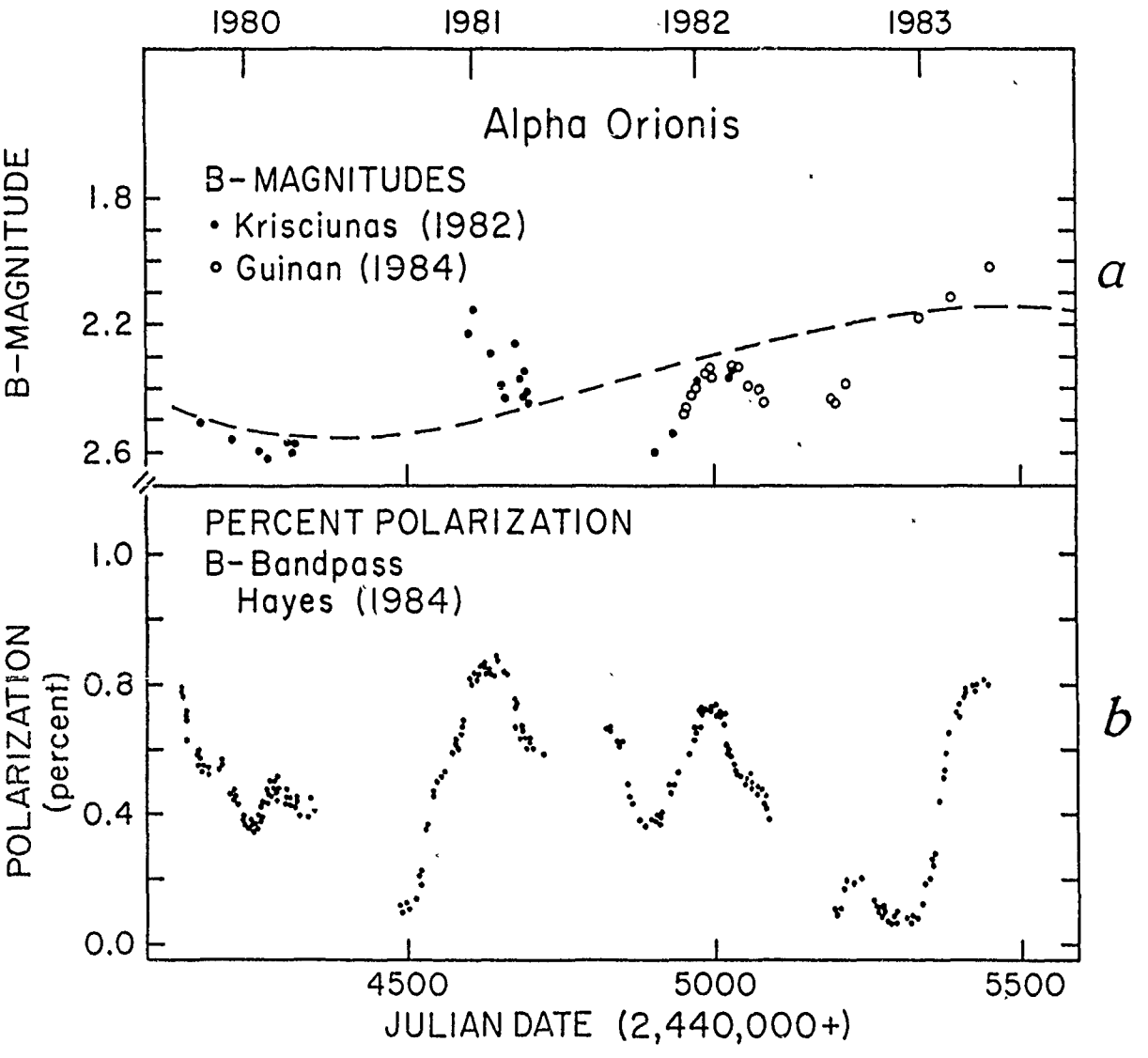
1980
1981
1982
1983
Alpha Orionis
B-MAGNITUDES
• Krisciunas (1982)
∘ Guinan (1984)
B-MAGNITUDE
1.8
2.2
2.6
a
PERCENT POLARIZATION
B-Bandpass
Hayes (1984)
POLARIZATION (percent)
1.0
0.8
0.4
0.0
b
4500
5000
5500
JULIAN DATE (2,440,000+)

Fig. 2

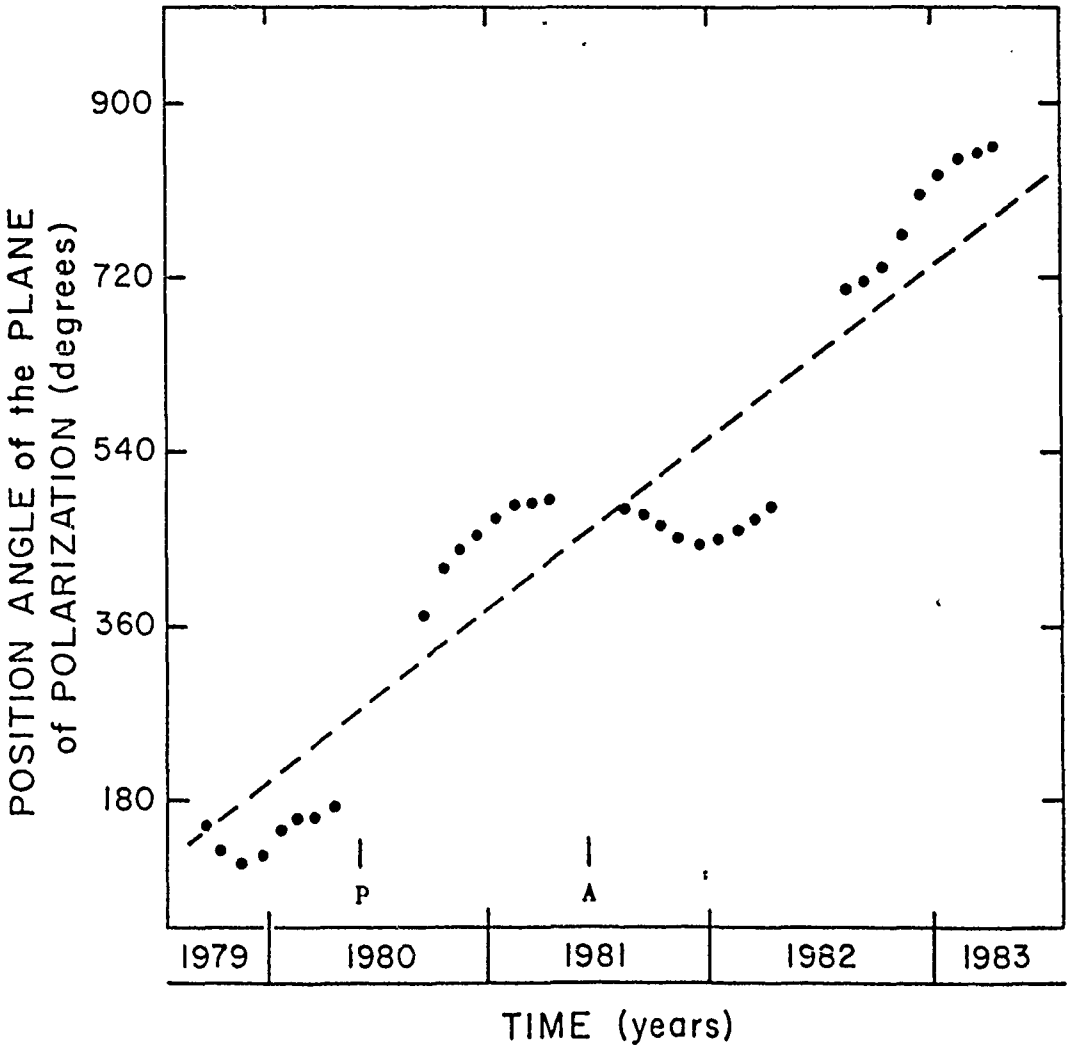
900
720
540
360
180
POSITION ANGLE of the PLANE
of POLARIZATION (degrees)
P
A
1979
1980
1981
1982
1983
TIME (years)

Fig. 3

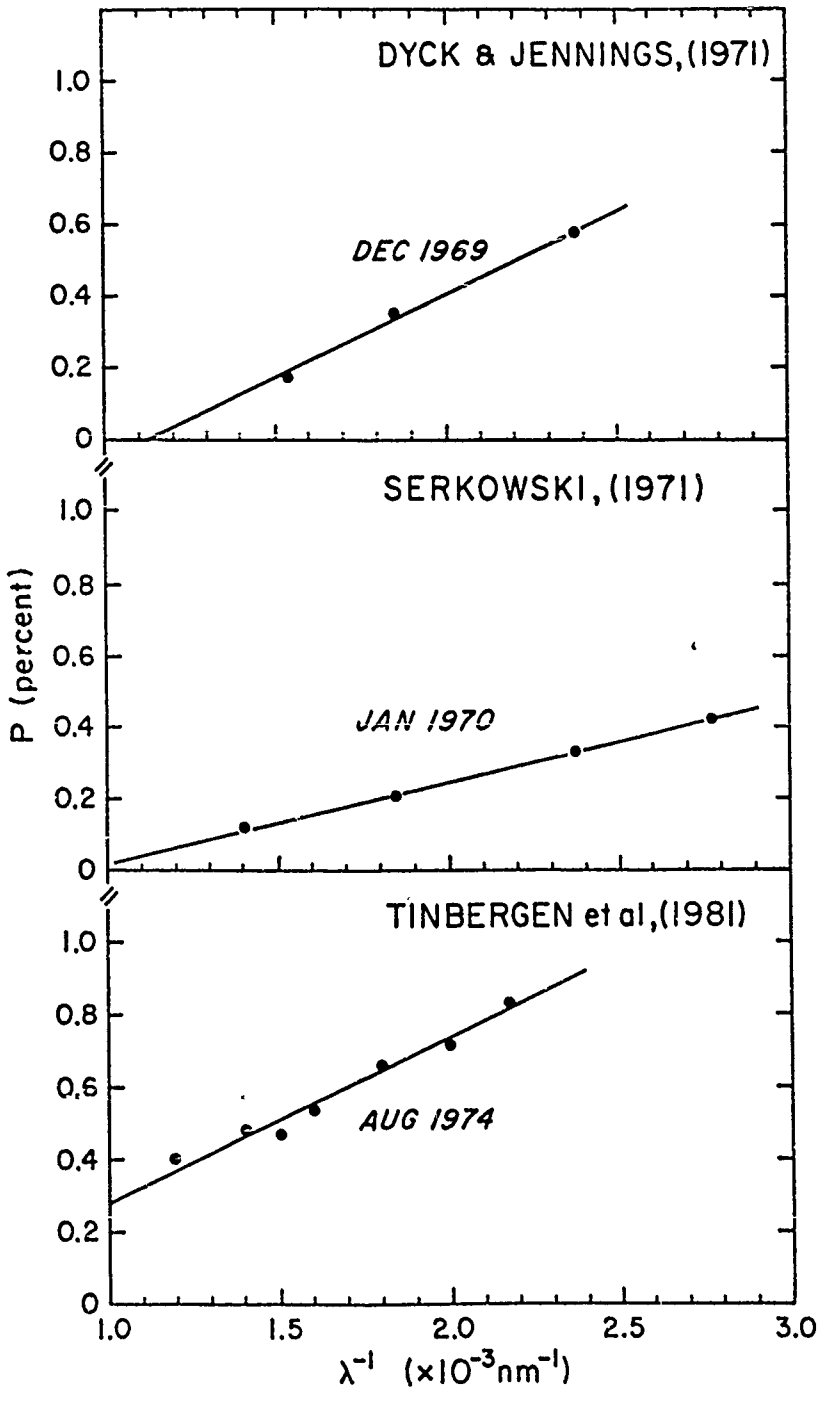
DYCK & JENNINGS, (1971)
DEC 1969
SERKOWSKI, (1971)
JAN 1970
TINBERGEN et al, (1981)
AUG 1974
P (percent)
λ⁻¹ (×10⁻³nm⁻¹)
0
0.2
0.4
0.6
0.8
1.0
1.5
2.0
2.5
3.0

Fig. 4

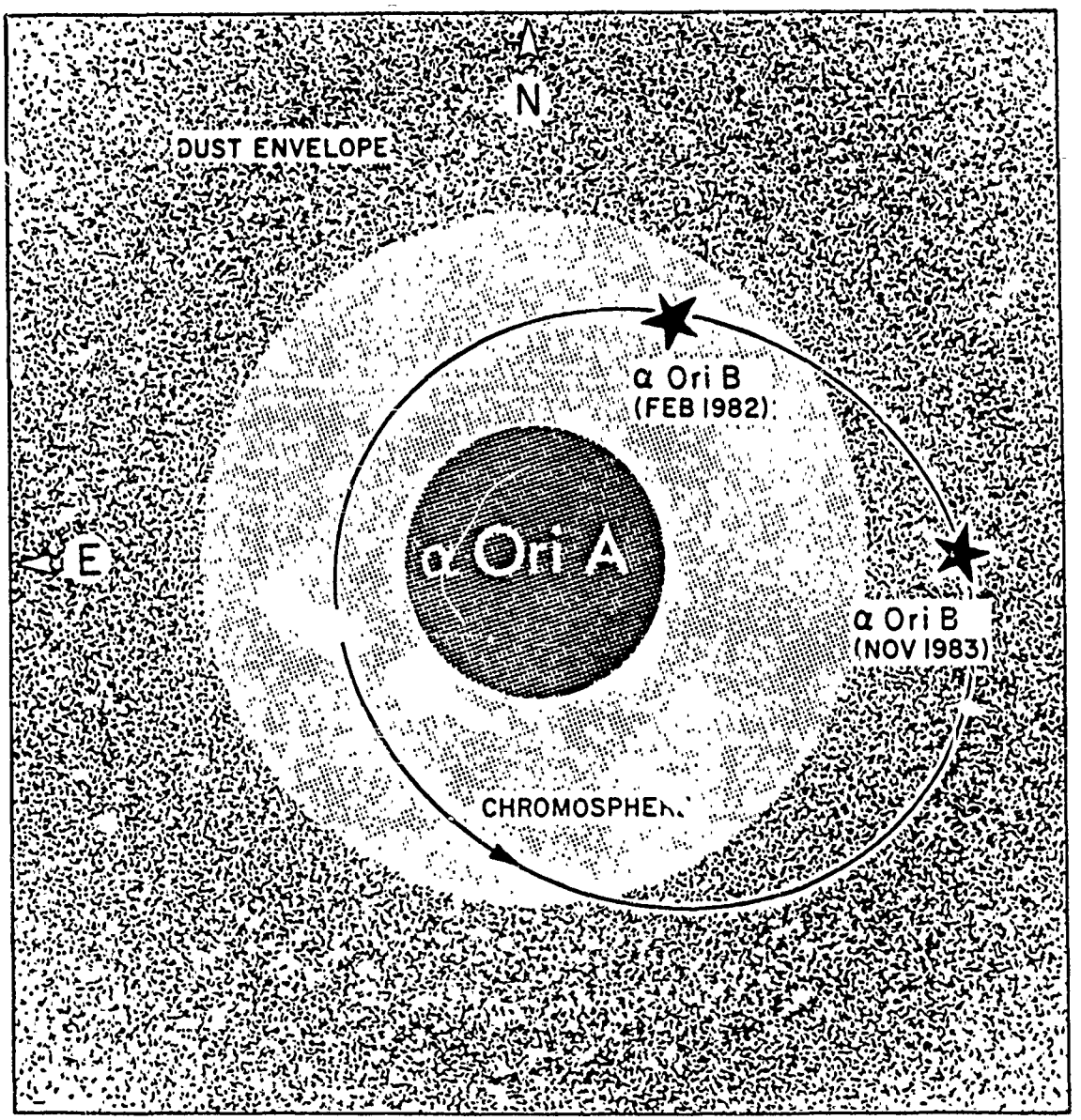
N
DUST ENVELOPE
α Ori B
(FEB 1982)
α Ori A
E
α Ori B
(NOV 1983)
CHROMOSPHERE

Fig. 5

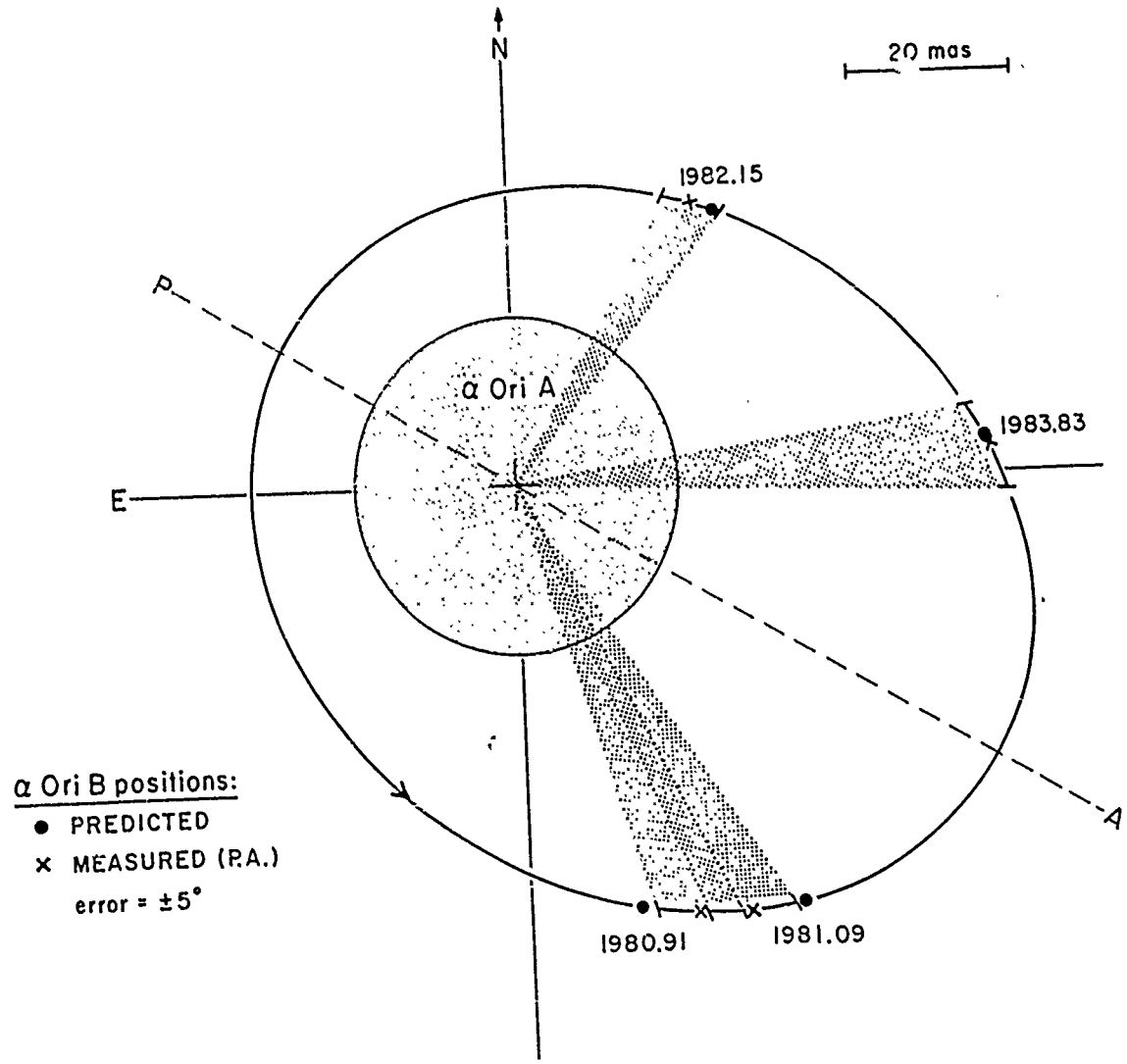
N
20 mas
1982.15
P
α Ori A
1983.83
E
A
α Ori B positions:
● PREDICTED
× MEASURED (P.A.)
error = ±5°
1980.91
1981.09

Fig. 6

APPENDIX
G

RESOLUTION OF THE HALO BINARY μ CAS IN THE OPTICAL

M. Karovska, P. Nisenson and R.V. Stachnik
Harvard-Smithsonian Center for Astrophysics
60 Garden St., Cambridge Ma. 02138

ABSTRACT

The faint secondary of the Population II binary system μ Cas has been detected at 850 nm, using a two-dimensional photon counting camera (the PAPA) and speckle imaging techniques. The reconstructed image of the μ Cas binary system permitted an unambiguous determination of the position angle (63° ± 2°) and separation ($1''.118 \pm 0''.023$) of μ Cas B, and its magnitude difference from the primary ($\Delta m \approx 5$ @ 850 nm). Using these results together with existing astrometric measurements, we estimated the masses of the components. Since errors in the mass estimates are still dominated by errors in the astrometric data, no definitive estimate of the helium abundance could be derived. However, using mean values for the masses and Z = 0.005 , we estimated Y = 0.21 for μ Cas A which is consistent with our estimate of the helium abundance for μ Cas B ($0.20 \leq Y \leq 0.25$).

I. INTRODUCTION

μ Cas is a Population II subdwarf, formed at an early stage in the evolution of the Galaxy and its chemical composition could reflect that of the early Universe. The primordial helium abundance is an important boundary condition for early universe cosmologies. The helium abundance of Population II dwarfs can not be determined spectroscopically, since the surface temperature is too low to permit excitation of the helium spectrum. Dennis (1965) suggested an alternative method of obtaining a helium abundance, using stellar interiors theory together with determinations of the star's mass and luminosity. Because μ Cas is a nearby binary system (d≈7.5 pc), many observational efforts have been directed towards the possibility of mass determination for the components.

Combining the existing astrometric orbital elements for this 22 year period binary with a single measurement of separation and magnitude difference was long held to permit a determination of the mass of the primary. With a maximum separation of an arcsecond and a very large luminosity ratio between the two components ($\Delta m_v > 6.5$), detection of the companion is extremely difficult at optical wavelengths. Earlier efforts to detect the secondary in the visual (cf. summary by Lippincott (1981)) reflect the difficulties of

obtaining an accurate determination of the position angle, separation and, especially, magnitude difference of μ Cas B with respect to the primary.

More recently, μ Cas B has been detected using one-dimensional infrared speckle interferometry (McCarthy, 1984). The smaller magnitude difference between the companion and the primary in the infrared, at 2.2 and 3.4 μm, permitted substantial improvement in estimates of the separation and apparent magnitudes. When these measurements were combined with the two most recently published sets of photocentric orbital elements and parallaxes (Lippincott, 1981 ; and Russell and Gatewood, 1983), they yielded two very different values for the mass of μ Cas A: 0.45 $M_\odot$ (using Lippincott results) and 0.89 $M_\odot$ (using Russell and Gatewood results). The estimated fractional helium abundance, based on the mass determined from the astrometric orbit (RG) is Y=0.25 ± 0.25.

Pierce and Lavery (1985) published results from selected short-exposure CCD images obtained at 1 μm. Their estimates of the μ Cas A mass were: 0.30 $M_\odot$ with elements from Lippincott (1981), and 0.61 $M_\odot$ with elements from Russell and Gatewood (1983). They adopted the value of 0.61 $M_\odot$ for the mass of μ Cas A and estimated the fractional helium abundance Y as Y=0.42 ± 0.30.

As pointed out by Faulkner (1971), the accuracy in the estimate of the fractional helium abundance required for

cosmological purposes is about 0.1. This implies a knowledge of the semi-major axes to within 3 - 4 %. Like McCarthy, Pierce and Lavery were led to the conclusion that the dominant source of errors in the deduced helium content are inaccuracies in the astrometric orbit. However, discrepencies between the two measurements leading to the substantial differences in the estimated value for the μ Cas A mass suggest that, in addition to improvement of the astrometric orbit, more accurate measurements of the position angle, separation and magnitude difference for μ Cas B are also required if a better estimate of the helium abundance is to be obtained.

We report here the first unambiguous speckle detection of μ Cas B at optical wavelengths (λ=850 nm). This faint source has been detected using the PAPA detector, a new two-dimensional photon counting camera (Papaliolios, et al., 1985), together with the techniques of speckle imaging. The potential of these techniques for detection of large magnitude difference companions has recently been demonstrated in the discovery of an optical companion to T Tauri (Nisenson et al, 1985) and in the detection of two companions to α Orionis (Karovska et al, 1986). The autocorrelation and image reconstructed from the μ Cas speckle data permitted an accurate determination of the position angle and distance of μ Cas B, and the inherent linearity and dynamic range of the PAPA photon counting camera permitted an accurate measurement of its apparent magnitude. These results were then applied to calculating an estimate of the helium abundance from μ Cas A and, for the first time, from μ Cas B.

II. OBSERVATIONS AND DATA PROCESSING

The speckle data on μ Cas were recorded on February 16, 1984 at the Cassegrain focus of the Multiple Mirror Telescope at Mt. Hopkins, Arizona. Though the telescope is normally operated with images from the six mirrors overlapped, for this data set only light from one 1.8 meter mirror was used. The PAPA camera was used with a foreoptics package built at the University of Arizona Steward Observatory by K. Hege and J. Beckers. This package provides magnification which matches the camera pixel scale to the telecope diffraction limit, as well as narrow band filters and correction for atmospheric dispersion. The camera records each detected photon as it arrives, so no shuttering is required at the telescope, and optimum exposure times (relative to the atmospheric time constant) are selected during data processing. For the data described here, a 5 millisecond exposure time gave optimal signal-to-noise in the reconstructions. The data were recorded using a 10 nm wide filter centered on 850 nm. Though the quantum efficiency of the extended-red S-20 photocathode in the PAPA drops substantially at this wavelength, it was still sufficent to obtain 20,000 counts per second from μ Cas. Data on a reference star which is unresolved at the telescope diffraction limit, θ Cas, were also recorded, immediately after the μ Cas observation. The data are stored by placing the digital photon addresses from the PAPA on

a video carrier and storing the result on video tape with a conventional VCR (Ebstein, 1984).

Data processing consists of binning the photon data into frames of the chosen exposure time, fourier transforming each frame, and then calculating the averaged power spectrum and complex autocorrelations needed for reconstruction. Details of the integration procedures and convergence rates are given in Nisenson and Papaliolios (1983). Both object and reference star data are integrated with the same parameters. The reference star data are then used in the reconstruction process for estimating the atmospheric transfer function and for deconvolution. After the speckle imaging reconstruction process, additional post-processing operations such as smoothing, filtering or application of techniques such as the Maximum Entropy Method may be applied to obtain signal-to-noise limited reconstructions.

III. RESULTS AND ANALYSIS

a. Observational Results

A very low contrast fringe pattern was detected in the power spectrum of μ Cas, indicating the presence of a second component. The secondary was also detected in the autocorrelation and in the

image reconstructed from this data set (Figure 1.). Since our technique of speckle imaging allows recovery of the phase as well as the amplitude in the fourier transform of the reconstructed image, it was possible to eliminate the 180° ambiguity normally associated with speckle interferometry and to determine the true position of μ Cas B. The resulting separation is 0.118 ± 0.023 arcsecond at a position angle of 63° ± 2°.

The unlimited dynamic range of the photon counting camera and its fundamental linearity give it a unique capability to measure large magnitude differences. This permitted accurate estimation of the magnitude difference with respect to the primary. At 850 nm the measured magnitude difference is 4.9 ± 0.2. Table 1 summarizes the results of this observation.

b. Mass Determination

The total mass of the system is given by Kepler's third law

$$M(A) + M(B) = \alpha^3 / \pi^3 P^2 \qquad (1)$$

where M(A) and M(B) are masses of μ Cas A and μ Cas B respectively, α is the angular semimajor axis of the orbit, π is the system's parallax and P is its orbital period.

The angular value of the unprojected semimajor axis of

the orbit can be calculated from the angular separation derived from the speckle observation, ρ , the predicted photocentric angular separation for the same epoch, ρ' , and the semimajor axis of the photocentric orbit, α'.

$$\alpha = (\rho / \rho') \alpha = R \alpha \qquad (2)$$

The ratio of measured angular separation to predicted photocentric separation gives the scale factor between the true and the photocentric orbit, R.

The fractional mass B = M(B) / (M(A) + M(B)) can be evaluated from the relation

$$B = R^{-1} + \beta \qquad (3)$$

if the fractional luminosity of the secondary β = L(B) / (L(A) + L(B)) is known (cf van de Kamp, 1981).

The mass ratio is now given by

$$M(A)/M(B) = B^{-1} - 1 \qquad (4)$$

The mass ratio combined with the system total mass yields the mass of the components.

Two recently published photocentric orbits (Lippincott, 1981, and Russell and Gatewood, 1983) provide the elements

needed to calculate the masses. A summary of the two sets of orbital parameters together with measured parallaxes is presented in Table 2. Throughout this paper, we will use the shorthand notation (L) for the Lippincott orbit/parallax and (RG) for the Russell and Gatewood orbit/parallax. In view of the differences between these two orbits (cf. McCarthy, 1984), elements from each were independently combined with our measurement of angular separation in order to calculate the masses. The measured magnitude difference between μ Cas A and μ Cas B at 850 nm ($\Delta m \approx 5$) suggests that the optical brightness of the secondary is negligible compared to the primary. Consequently, the fractional luminosity β can be neglected in equation (3).

Using the elements from (L) the calculated orbital scale factor and masses of μ Cas A and μ Cas B are

$R = 4.7 \pm 0.1$

$M(A) = 0.49\ M_\odot \pm 0.06$

$M(B) = 0.13\ M_\odot \pm 0.02$

The scale factor and masses derived using (RG) and the orbital parameters and parallax are

$R = 5.7 \pm 0.4$

$M(A)=0.82\ M_{\odot} \pm 0.23$

$M(B)=0.18\ M_{\odot} \pm 0.05$

IV. DISCUSSION

a. Comprison With Other Observations

The reconstructed image of the μ Cas binary system permitted unambiguous determination of the position angle of the secondary. The measured position angle is consistent (within the error bars) with the predicted position angles for μ Cas B from both published photocentric orbits (Table 3). The difference between the position angle predicted from the (RG) orbit and the position angle determined by McCarthy (1984) and by Pierce and Lavery (1985) are respectively, 17° and 26°.

Two scaling factors for the photocentric orbit derived from our measurement of the separation of μ Cas B combined with (L) and (RG) sets of astrometric elements, are in excellent agreement with those calculated by McCarthy (1984). They are also consistent, within the published error bars, with the results given by Pierce and Lavery (1985) (see Table 3). The estimated errors in our results are comparable to the errors calculated by McCarthy. While these errors are large, they are mainly due to the uncertainities in the parameters of the

photocentric orbit. As has been pointed out by Russell and Gatewood (1983), the apparent higher accuracy in Lippincott's orbital elements, and consequently, of the scale factor estimate based on these elements, may be due to an underestimate of the actual errors.

Differences between the two sets of astrometric elements yielded a substantial inconsistancy in values computed for the masses of the two components. Masses of μ Cas A and μ Cas B determined using (RG) orbital elements are about 30-40% higher than the masses estimated using Lippincott's elements. Additionally, the accuracy in mass determination is strongly affected by uncertainities in scale factors as well as in parallaxes.

This discussion leads to the conclusion that an improvement of the astrometric parameters is a necessary condition for more accurate determination of the masses. However, we made an attempt at discrimination between the two astrometric orbits by comparing masses calculated for μ Cas A with the mass which would be expected in view of its luminosity were it a main-sequence star.

b. Luminosity of μ Cas A and μ Cas B

The bolometric luminosity of μ Cas A can be calculated from its apparent magnitude, bolometric correction and parallax. A bolometric correction for μ Cas A has been determined by

Carney and Aaronson (1979),(BC=-0.22), by using UBVRIJHK photometry and model atmosphere calculations for population II subdwarfs. The μ Cas A apparent magnitude is m_v=5.16 assuming that there is no contribution of light from the secondary. The apparent magnitude and bolometric correction combined with the two independent parallax measurements [π=0.132 arcsec (L), and π=0.1368 (RG)] yield the bolometric luminosities of μ Cas A of 0.48 $L_\odot$ and 0.45 $L_\odot$, respectively.

We applied the empirical mass-luminosity relationship (Smith, 1983) in order to make an estimate of the μ Cas A mass. Masses which correspond to luminosities of 0.48 $L_\odot$ and 0.45 $L_\odot$ are respectively, 0.83 $M_\odot$ and 0.82 $M_\odot$. These estimates are consistent with the mass of 0.82$_\odot$ determined using (RG) results. For a main-sequence star having a mass of 0.49 $M_\odot$ (the mass of μ Cas A estimated from (L)), the expected luminosity would be 0.05 $L_\odot$. This luminosity would imply an effective temperature for μ Cas A of more than 1000 degrees lower than the effective temperature of about 5200 K which is derived for this star by several authors (Strom and Strom, 1967; Carney and Aaronson, 1979; Tomkin and Lambert, 1980). If, however, μ Cas A has a mass of about 0.5 $M_\odot$ and its luminosity is about 0.45 $L_\odot$, then the conclusion would be that it exhibits a substantial overluminosity when compared to similar stars. These values may, for example, be compared to those for the primary of the visual and astrometric binary 85 Peg AB having a mass of 0.82 $M_\odot$ $\pm$0.23 (Lippincott, 1981b) and luminosity of 0.69 $L_\odot$(Carney and Aaronson, 1979)).

Since the mass of 0.82 $M_\odot$ (calculated from the (RG) orbit and parallax) seems to be more appropriate for μ Cas A then the mass of 0.49 $M_\odot$ (calculated using (L)), we adopted the value of 0.18 $M_\odot$ (RG) for μ Cas B in order to derive its bolometric luminosity. From the mass-luminosity relationship for low mass stars (Veder, 1973), the mass of 0.18 $M_\odot$ indicates a bolometric luminosity of about 0.004 $L_\odot$. Using results from UBVRIJHKL photometry for some of the single halo subdawarfs of similar luminosity (Table A-I, Veeder, 1974) and from UBVRIJHK photometry of μ Cas A (Carney and Aaronson, 1979) together with the measured magnitude difference between the two stars at 850 nm ($\Delta m \approx 5$), we estimated a magnitude difference of about 7 at 550 nm. This value is about 1.5 magnitude larger then the magnitude difference measured by Wickes and Dicke (1974) but is in agreement with the magnitude difference calculated by McCarthy (1984). McCarthy estimated a magnitude difference of about 6.5 between the two components using the 2.2 μm absolute magnitude of μ Cas B and the mass calculated from Russ ll and Gatewood's astrometric elements together with Veder's (1984) studies of M dwarf stars. He concluded that the masses calculated using (L) are implausible since the two components would be overluminous when compared to main-sequence models.

This analysis suggests that the masses derived for μ Cas A and μ Cas B using the (RG) astrometric results may be more appropriate. However, these results are by no means definitive, since in our analysis, we did not take into account errors in

the mass estimate. In fact, they are substantial and can not be ignored in a luminosity calculation, and especially in a helium abundance determination, where the errors are comparable with the result itself (cf. McCarthy, 1984; Pierce and Lavery, 1985)

c. Helium abundance

As has been suggested by Dennis (1965), the helium abundance of μ Cas A can be determined using stellar interiors theory, only if its mass, luminosity, heavy element abundance and age are accurately known. Unfortunately, at present the inaccuracies in the mass and luminosity of μ Cas A are large and there are several different estimates of heavy element abundance. Dennis (1965) calculated helium abundances of μ Cas A for two assumptions as to its heavy element abundance: Z=0.005 and Z=0.015. A heavy element abundance of about 0.005 has been estimated by several authors (Catchpole et al., 1967; Cohen, 1968; Carney and Aaronson, 1979). More recently, Tomkin and Lambert derived an even lower value (≈0.00[illegible].

Determination of the age of μ Cas A is also difficult. If its mass is as high as 0.8 $M_\odot$ or even higher, then it would be uncertain whether the star is still on the zero-age main sequence (ZAMS). It is difficult to estimate the time elapsed since the ZAMS phase. The problem of age determination can be overcome if instead of using μ Cas A for the helium abundance determination one uses μ Cas B. Since the mass of this star is

very small it is certain that it could not have evolved from the ZAMS.

We made an attempt to determine helium abundance for μ Cas A and for μ Cas B by assuming that both stars have the same age and same heavy element abundance (Z=0.005). For our calculations, we adopted masses of 0.82 $M_\odot$ and 0.18 $M_\odot$, respectively, for μ Cas A and μ Cas B.

Assuming 0.45 $L_\odot$ for the luminosity of μ Cas A, 5260 K for its effective temperature (derived from model-atmosphere calculations, Carney and Aaronson (1979)), and a value of 0.005 for the heavy element abundance, we interpolated between the evolutionary models of Mengel at al. (1979) in order to estimate the helium abundance. The derived helium abundance is 0.2. We obtained a nearly identical abundance (Y=0.21) by applying Dennis' (1965) interpolation formula

$$m = 1.52\ (X+0.60)^{86/59}\ (Z+0.0104)^{14/59}\ (1+X)^{7/59}\ X^{4/59}\ L^{11/59}$$

Here, m is the mass of the star, L its luminosity, X and Z, respectively, hydrogen and heavy element abundances.

In order to estimate the helium abundandance of μ Cas B we assumed 0.004 $L_\odot$ for its luminosity, 0.18 $M_\odot$ for its mass and 0.005 for its heavy element abundance and interpolated between the theoretical stellar models for the lower end of the main sequence (VandenBerg, 1983). The estimated helium abundance is

between 0.20 and 0.25.

Although these two estimates seem to be consistent, it is premature to form any definitive conclusions about the real helium abundance of these two stars. Unambiguous determination of the helium abundance will be possible only with improved knowledge of the masses of the components and of their heavy element content.

V. CONCLUSION

This work demonstrates that at this point the accuracy in the mass determination of the components and consequently in estimation if the helium abundance of μ Cas A and μ Cas B is strictly constrained by uncertainities in the orbital parameters and the parallax. In view of the 22 year orbital period of this binary, improvement of the photocentric parameters in the next few years seems unlikely. However, we believe that the uncertainities in the astrometric orbit can be reduced independently of astrometric measurements by additional direct measurement of the position angle and angular separation of μ Cas B in the optical as well as at infrared wavelengths. The fact that the secondary is now approaching apoastron (middle of 1986) suggests that these measurement can be done with high precision. Within the next few years, we expect to obtain a

series of measurements of μ Cas B position angle and separation which should provide additional constraints on the orbital parameters. We expect that these measurements, together with new determinations of parallax which should come from Hipparchos or Space Telescope observations, will allow an accurate estimate of the masses of the components and consequently, of the helium abundances of μ Cas A and μ Cas B.

ACKNOWLEDGEMENTS

We wish to thank C. Papaliolios, S. Ebstein, J. Beckers and K. Hege for their assistance with the observations. We are grateful to P. Demarque, B. Carney and R. Noyes for many helpful discussions. We acknowledge the ongoing support of M. Radoski of the Air Force Office of Scientific Research. This work was funded under grant no. AFOSR-81-0055 from AFOSR.

Table 1

θ	$63° \pm 2°$
ρ	$1''.118 \pm 0''.023$
Δ m	4.9 ± 0.2

Table 2

Orbit	α'' (")	P (yr)	T	e	i (°)	Ω (°)	ω (°)	π (")
L	0.186	21.43	1954.34	0.61	109.5	47.4	335.9	0.132
	±0.001	±0.05	±0.08	±0.02				±0.002
RG	0.1900	22.09	1931.60	0.58	108.2	47.4	324.8	0.1368
	±0.0038	±0.26	±0.07	±0.03				±0.005

Table 3

Epoch	*Orbit*	*Scale Factor*	*Position angle difference*	*References*
1983.20	L	4.6±0.2	9° ± 2	McCarthy
	RG	5.7±0.4	17° ± 6	(1984)
1983.5	L	4.2±0.3	19° ± 3	Pierce & Lavery
	RG	5.2±0.6	26° ± 7	(1985
1984.13	L	4.7±0.1	2° ± 3	This work
	RG	5.7±0.4	5° ± 6	

REFERENCES

Carney, B.W., and Aaronson, M. 1979, *Astr. J.*, **84**, 867.

Catchpole, R.M., Pagel, B.E.J., and Powell, A.L.T. 1967, *M.N.R.A.S.*, **136**, 403.

Cohen, J.G. 1968, *Ap. J.*, **153**, 179.

Dennis, T.R. 1965, *P.A.S.P.*, **77**, 283.

Ebstein, S. 1984, *Rev. Sci. Instrum.*, **54**, 883.

Faulkner, J. 1971, *Phys. Rev. Lett.*, **27**, 206.

Kamp, van de, P. 1981, *Stellar Paths* (Reidel, Dordrecht).

Karovska, M., Nisenson, P., Noyes, R., and Roddier, F. 1986, *Ap. J.*, (to be published)

Lippincott, S.L. 1981a, *P.A.S.P.*, **93**, 376.

Lippincott, S.L. 1981b, *Ap. J.*, 248.

McCarthy, D.W. 1984, *Astron. J.*, **89**, 433.

Mengel, J.D., Sweigart, A.V., Demarque, P., and Gross, P.G. 1979, *Ap. J. Suppl.*, **40**, 733.

Nisenson, P., and Papaliolios, C. 1983, *Optics Comm.*, **47**,91.

Nisenson, P., Stachnik, R.V., Karovska, M., and Noyes, R. 1985, *Ap. J. (Letters)*, **297**, L17.

Papaliolios, C., Nisenson, P., and Ebstein, S. 1985, *Appl. Opt.*, 24, 287.

Pierce, M.J., and Lavery, R.J. 1985, *Astron J.*, 90, 647.

Russell, J.L., and Gatewood, G. 1984, *P.A.S.P.*, 96, 429.

Smith, P.C. 1983, *Observatory*, 103, 29.

Strom, S.E., and Strom, K.M. 1967, *Ap. J.*, 150, 501.

Tomkin, J., and Lambert, D.L. 1980,*Ap. J.*, 235, 925.

Veeder, G. 1974, *Astron. J.*, 79, 1056.